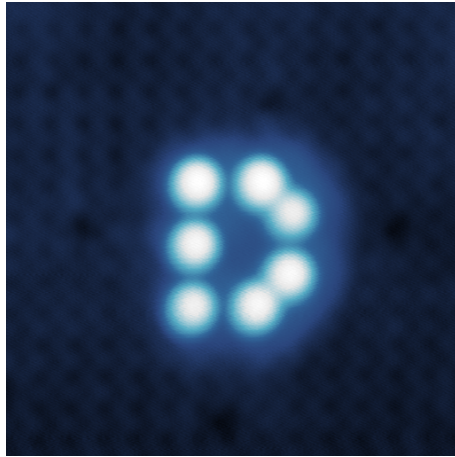


Frustrated spin chains on a square lattice

Delft University of Technology



Shang-Jen Wang

Supervisors:

J. Gobeil and Prof. Dr. A.F. Otte

Master thesis

2018

Abstract

This thesis investigates intrinsic frustrated magnetic systems on an insulating square lattice. The frustrated systems were successfully engineered from magnetic iron atoms on top of an insulating square $c(2 \times 2)$ reconstruction of nitrogen on $\text{Cu}_3\text{Au}(100)$ (copper-gold) surface. Vertical atom manipulation was used to position the magnetic atoms atomically precise on the surface and methods were found to increase the success rate of this. For the investigation of frustration, a numerical simulator was made in Python for modelling frustrated spin structures based on already existing spin models and the following experimental measurements were taken: topography, spectroscopy and current-time traces. The simulations of a frustrated spin system show low energy excited states and the measurements show switching of the system between states.

Contents

1	Introduction	6
2	Theory	8
2.1	The Hamiltonian	8
2.1.1	The Heisenberg model	8
2.1.2	Anisotropy and Zeeman Hamiltonian	10
2.2	Analysis of Eigenvectors	11
2.3	Frustrated systems	12
2.4	IETS: Inelastic Electron Tunneling Spectroscopy	15
3	Numerical simulation methods	17
3.1	The Hamiltonian	17
3.2	Expectation values	19
4	Experimental methods	20
4.1	Scanning tunneling microscope	20
4.1.1	Unisoku USM1300	20
4.1.2	Sample preparation of Cu_3AuN_2	22
4.1.3	Topography	24
4.1.4	Spectroscopy	24
4.1.5	Spin-polarized STM	26
4.1.6	ESR: Electron spin resonance	27
4.2	Single atom manipulation	28
4.2.1	Vertical atom manipulation	29
4.2.2	Vertical atom manipulation on Cu_2N	30
5	Results	32
5.1	Numerical simulation results	32
5.1.1	Single atom (verification)	32
5.1.2	Trimer (verification)	34
5.1.3	A frustrated 7 atom structure: D7	36
5.1.4	A frustrated 9 atom structure: D9	40
5.1.5	ESR	43
5.2	Experimental results	44

5.2.1	Atom manipulation process and built structures.	44
5.2.2	Measurements of a frustrated D7 structure	46
5.3	Comparison of Simulation and Experimental Results	52
6	Conclusion and Outlook	53

List of Figures

2.1	The six possible ground states of the antiferromagnetic Ising model on an equilateral triangle. The red line indicates the frustrated ferromagnetic coupled pair.	13
2.2	(a) Schematic of Cu_2N lattice, where Cu is the bigger yellow circle and N is the smaller blue circle. The coordinate system is determined with respect to the adatom (red sphere), z is along N-direction, x is along hollow-direction and y is out-of-plane direction. Figure adapted from [1]. (b) The different couplings between adatoms according to the angle and distance between them. J_1 is along the N direction and is antiferromagnetic, J_2 is along the hollow direction is antiferromagnetic but weaker than J_1 and J_3 is ferromagnetic. (c) The different couplings, but now the Cu_2N background is removed for simplification.	14
2.3	The smallest frustrated system on a square lattice, where J_1 is antiferromagnetic and J_3 is ferromagnetic, and $ J_1 \approx J_3 $	14
2.4	The ‘D’ structure, where J_1, J_2 are antiferromagnetic and J_3 is ferromagnetic, and $ J_1 \approx J_3 , J_2 < J_1 $. In the right panel an example of one of the 4 degenerate ground states, the frustration is indicated in red.	15
2.5	General process of tunneling in an STM. The adatom starts in the ground state, an electron tunnels through the barrier putting the adatom in a virtual state and finally the adatom relaxes to the ground state (elastic tunneling) or excited state (inelastic tunneling). In the inelastic tunneling case the magnetization has changed. Image adapted from reference [1]	16
3.1	The number of coupling terms that need to be taken into account differs for a quasi-one dimensional system (a) and a two dimensional system (b) . In (a) the number of coupling terms won’t exceed the number of atoms. In (b) a single atom can have more than two couplings and thus the amount of coupling terms can be quite large making book keeping difficult.	18

4.1	<p>(a) A picture of the Unisoku UMS 1300. The system is on top of a floating table in order to reduce vibrations, where the three vacuum chambers on top of the table and the green cryostat (also floating) is under the table. (b) Schematic of the cryostat from the STM. The absorption pump is for condensing ^3He, the 1 K pot houses the ^4He, the SC Magnet is used to create an external field and the STM unit houses the STM-tip and sample. The image was taken from the Unisoku USM 1300 website.</p>	21
4.2	<p>Topography images of the three sample preparation stages: (a) clean $\text{Cu}_3\text{Au}(100)$ after annealing and sputtering, (b) insulating N islands on $\text{Cu}_3\text{Au}(100)$ and (c) Evaporated Fe atoms on $\text{Cu}_3\text{Au}(100) - c(2 \times 2)\text{N}$. The nitrogen islands, visible in (b) and (c), are the darker patches surrounded by the brighter area and the Fe atoms are the white dots in (c). The images were taken at 1 K, (a) 500 pA and 300 mV, (b) 20pA and 100 mV and (c) 20 pA and 50 mV.</p>	23
4.3	<p>Schematics of the two scanning modes, the top panel shows constant height mode and the bottom panel shows constant current mode. . .</p>	24
4.4	<p>(a) The spectroscopy of a single Fe atom on Cu_3AuN_2 using the lock-in-amplifier taken at 330 mK and a setpoint of 20 mV and 1 nA. (b) Shows the way the lock-in-amplifier acquires the dI/dV, the amplitude of the incoming sine wave is determined by V_{mod}.</p>	25
4.5	<p>(a) Schematic of spin-polarized imaging. The tip has a single atom at the apex and the tunnel current will be higher or lower depending on the alignment of the adatom. Image adapted from [1]. (b) A topography of an antiferromagnetic structure made from Fe atoms on Cu_3AuN_2 taken with a spin-polarized tip at 50pA, 2 mV, 1 T and 330 mK. The difference in tunnel current is translated into a difference in size. The tip is polarized by applying a B-field along the easy-axis of Fe. (c) A Spectroscopy of a single Fe atom on Cu_3AuN_2 taken with a spin-polarized tip at 1 T, 330 mK and a setpoint of 1 nA and 1 T. The difference in tunnel current translates to the left half having a higher conductance than the right half.</p>	26
4.6	<p>(a) Linear crystal field splitting on Fe, where a magnetic field B_z splits state $0\rangle$ and $1\rangle$. The image idea taken from reference [2]. (b)The RF chopping scheme for a lock-in measurement, the tunnel current is higher when RF is turned on.</p>	28
4.7	<p>The schematic of picking up an atom explained by the double potential well. In (1) the tip is within imaging distance and the atom is still stable on the surface. As the tip gets closer the potential well gets distorted (2). Applying a bias voltage will favor the potential well of the tip and the atom will fall into it (3). When the tip is moved the atom will follow and the atom is picked up (4). Image adapted from reference [1]</p>	30

4.8	A visualization of vertical atom manipulation on Cu_2N lattice. (a) The Fe atom is in the lowest energy configuration sitting on top of a Cu atom and having two covalent bonds with the neighbouring N. (b) A bias voltage is applied breaking the covalent bonds of the Fe atom and the tip picks it up. (c) After being dropped off from the tip the Fe atom lands on a N atom forming a single covalent bond and leaving a single unpaired electron. In (d) the atom has hopped from the N atom to the Cu atom and forming two covalent bonds bringing it back to the lowest energy configuration. Images adapted from reference [1]	31
5.1	The evolution of the excitation energies with respect to field for a single Fe atom on Cu_2N . Here B_z is chosen along N direction (c) , B_x is chosen along the hollow direction (a) and B_y is chosen along the out-of-plane direction (b)	33
5.2	Visualization of the studied trimer. It is an open ended chain consisting of three atoms antiferromagnetically coupled with the N direction coupling J_1	34
5.3	The population of the individual atoms for the first two eigenstates with corresponding eigenenergies of a Fe-trimer on a Cu_2N lattice at $B = 0$ T along N direction, the parameters used can be found in Table 5.1. The eigenstates are displayed for (a) the full crystal field, (b) when $D = 0$, (c) when $E = 0$ and (d) when $D, E = 0$. The representation idea was taken from reference [3].	35
5.4	The population of the individual atoms for the first two eigenstates with corresponding eigenenergies of a Fe-trimer on a Cu_2N lattice at $B = 500$ mT along N direction, the parameters used can be found in Table 5.1. The eigenstates are displayed for (a) the full crystal field, (b) when $D = 0$, (c) when $E = 0$ and (d) when $D, E = 0$	36
5.5	Visualization of the magnetically frustrated D7. It is a closed chain consisting of 7 atoms both antiferromagnetically (J_1 and J_2) and ferromagnetically (J_3) coupled according to the orientation of the atoms. The values for the couplings can be found in Table 5.1.	37
5.6	The population of the individual atoms for the first four eigenstates with corresponding eigenenergies of a Fe-D7 on a Cu_2 lattice at $B = 0$ T. The white space separating atom ‘C’ and ‘D’ is to indicate the weak coupling, which is also present between atom ‘G’ and ‘A’.	37
5.7	The population of the individual atoms for the first four eigenstates with corresponding eigenenergies of a Fe-D7 on a Cu_2 lattice at $B = 500$ mT. The white space separating atom ‘C’ and ‘D’ is to indicate the weak coupling, which is also present between atom ‘G’ and ‘A’.	38

5.8	The population of the individual atoms for the first four eigenstates with corresponding eigenenergies of a Fe-D7 on a Cu ₂ lattice at $B = 0$ T. On atom ‘D’ an anisotropy parameter of $D = -1.519$ meV was used. The white space separating atom ‘C’ and ‘D’ is to indicate the weak coupling, which is also present between atom ‘G’ and ‘A’.	39
5.9	The B-field required to counterbalance the effect of the varying anisotropy on atom ‘D’.	40
5.10	Visualization of the magnetically frustrated D9, it is a closed chain consisting of 9 atoms both antiferromagnetically (J_1 and J_2) and ferromagnetically (J_3) coupled according to the orientation of the atoms. The values for the couplings can be found in Table 5.1.	41
5.11	The population of the individual atoms for the first four eigenstates with corresponding eigenenergies of a Fe-D9 on a Cu ₂ lattice at $B = 0$ mT. The white space separating atoms ‘C-D-E’ and atoms ‘H-I-A’ is to indicate the weak coupling.	41
5.12	The population of the individual atoms for the first four eigenstates with corresponding eigenenergies of a Fe-D9 on a Cu ₂ lattice at $B = 500$ mT. The white space separating atoms ‘C-D-E’ and atoms ‘H-I-A’ is to indicate the weak coupling.	42
5.13	The population of the individual atoms for the first four eigenstates with corresponding eigenenergies of a Fe-D9 on a Cu ₂ lattice at $B = 500$ mT. On atom ‘D’ an anisotropy parameter of $D = -1.519$ meV was used. The white space separating atoms ‘C-D-E’ and atoms ‘H-I-A’ is to indicate the weak coupling.	43
5.14	The frequency needed to excite the trimer from the ground state to the first excited state at a global B_z -field of 1 T on the blue atoms and a tip induced field sweep on the red atom.	44
5.15	Images of spin structures made from Fe atoms, assembled through vertical atom manipulation and located on a $\sim 40 \times 30$ nm ² and $\sim 30 \times 30$ nm ² nitrogen island. (a) The 5 chain and 4 x 2 structures as in [4]. (b) The frustrated D7. Both images taken at 50 mV and 50 pA.	45
5.16	Images of the built spin structures made from Fe atoms and assembled through vertical atom manipulation. (a) 3 atom chain (trimer), (b) 5 atom chain, (c) 4 x 2, (d) Frustrated D7, (e) horizontal frustrated D9 and (f) vertical frustrated D9. Images taken at 50 pA and (a) , (b) , (c) 50 mV and (d) , (e) , (f) 20 mV	46
5.17	Images taken with a spin-polarized tip of the D7 structure at 1 T, 2 mV and (a) 50 pA, (b) 100 pA, (c) 150 pA, (d) 200 pA. The naming scheme of the atoms is visible in (a) . Notice the shadow occurring at higher setpoints in atoms ‘D’ and ‘E’	47

5.18	Spin-polarized spectroscopy of the individual atoms from a D7 at 1 T and a setpoint of 20 mV and (a) 500 pA, (b) 1 nA. The naming scheme in the legend follows the one in Figure 5.17a and the color scheme follows the different sections of the D7. There are two lines at 2 mV and 3 mV indicating the first excitation for atom ‘D’ and ‘E’.	48
5.19	Normalized current time traces taken with a spin-polarized tip at 3 mV and 1 T for atoms ‘A’ and ‘E’. The title contains the current setpoint and each row is labeled by the corresponding atom. The current is centered around the setpoint and for atom ‘A’ at 200 pA, the y-axis should be read as $y \in [199.8, 200.2]$ pA	49
5.20	Normalized histograms of the current versus time taken with a spin-polarized tip at 3 mV and 1 T for atoms ‘A’, ‘B’ and ‘C’. The title contains the current setpoint and each row is labeled by the corresponding atom. The histogram is centered and for atom ‘A’ at 50 pA, the x-axis should be read as $x \in [49.7, 50.3]$ pA	50
5.21	Normalized and centered histograms of the current versus time taken with a spin-polarized tip at 3 mV and 1 T for atoms ‘D’ and ‘E’. The title contains the current setpoint and each row is labeled by the corresponding atom.	51
5.22	Normalized and centered histograms of the current versus time taken with a spin-polarized tip at 3 mV and 1 T for atoms ‘F’ and ‘G’. The title contains the current setpoint and each row is labeled by the corresponding atom.	51

Chapter 1

Introduction

A quantum spin liquid (QSL) is a collective spin state in which the interacting spins, much like the molecules in a liquid, are disordered and remain this way down to absolute zero [5]. QSL was first introduced by Anderson [6] in 1973, proposing that it describes the ground state for an antiferromagnetic spin system on a triangular lattice. An interest in QSL's started to generate in 1987 when Anderson [7] proposed a theory that superconductivity could emerge by doping a QSL. One way to emerge a QSL is by intrinsic magnetic frustration. Frustration occurs when it is impossible to simultaneously satisfy two competing forces and this leads to exotic properties [5]. In magnetic crystals they are known to have massive intrinsic degeneracy of the ground state. A simple spin system containing frustration is the antiferromagnetically coupled Ising model in a triangle and has been done on a hexagonal lattice [8]. This was built directly on the metallic crystal and causes coupling between the spin system and the conduction electrons in the metal.

In this thesis a focus lies on building frustrated magnetic systems on a lattice that has an insulating layer in order to decouple the spin system and the conduction electrons. The spin system will be made from magnetic iron (Fe) adatoms, which are evaporated on a square $c(2 \times 2)$ reconstruction of nitrogen, acting as an insulating monolayer, on $\text{Cu}_3\text{Au}(100)$ (copper-gold). This research project has two objectives, the first was to create a numerical simulator in the programming language Python that will be used to predict the eigenstates and energies of frustrated spin structures. The simulator is based on already existing spin models: Heisenberg model, anisotropy Hamiltonian and Zeeman effect. The eigenenergies and eigenstates of the spin systems are calculated by an exact diagonalization method. This simulator will also be used in the future by the ottelab group in order to study various spin structures. The second is to build and explore intrinsic magnetic frustration. The structures were built in a scanning tunneling microscope (STM) using vertical atom manipulation and studying the properties was done with topography, inelastic electron tunneling spectroscopy, current-time traces and spin-polarized STM.

The thesis presents simulations of frustrated systems, which show the population of each individual atom in the spin states along the z-axis. The frustrated systems show low energy excited states, indicating intrinsic degeneracy of the ground state. The frustrated spin structures were successfully engineered on a square lattice. Vertical atom manipulation on copper-gold-nitride shows the same behaviour as on the more commonly used copper-nitride surface and methods were found to improve the success rate. Experimental measurements on the frustrated systems show switching of the system between states in the form of telegraphic noise. This also indicates low energy excited states.

The thesis starts with a discussion of the theoretical background in chapter 2, followed by the methods for the numerical simulations in chapter 3 and the methods for all the experimental work in chapter 4. The results in chapter 5 are split up in three sections, first covering the numerical simulations, followed by the experimental results and the comparison of the two. Lastly chapter 6 will present the conclusion and outlook for follow up research.

Chapter 2

Theory

This chapter will contain a description of the theoretical models in order to simulate the experimental sample in section 2.1. This will be followed by section 2.2 covering the analysis of the eigenstates in order to extract the populations of the individual atoms. Section 2.3 will present a detailed description of the frustrated system. Lastly section 2.4 will cover the involved physics in a spin excitation measurement performed in an STM.

2.1 The Hamiltonian

The Hamiltonians that are used to simulate the sample are: the Heisenberg Hamiltonian for neighbouring spin interaction, the anisotropy Hamiltonian to simulate the magnetic anisotropy induced by the surface and the Zeeman effect to split the spin states.

2.1.1 The Heisenberg model

The Heisenberg model describes the exchange interaction between neighbouring spins of a magnetic system. In this thesis only the nearest neighbour interaction and quasi-one dimensional systems are considered. The Heisenberg Hamiltonian for a one dimensional chain, where index i indicates the i^{th} atom, is [9]:

$$\hat{H}_{Heis} = \sum_{i=1}^N J_{i,i+1} \hat{\mathbf{S}}_i \cdot \hat{\mathbf{S}}_{i+1}. \quad (2.1)$$

The Heisenberg model is subject to a periodic boundary condition where $\hat{\mathbf{S}}_{N+1} = \hat{\mathbf{S}}_1$, since the systems considered are one dimensional chains.

J is the coupling constant between two atoms, where the magnitude and sign are dependent on the distance and orientation of the two atoms [10]. The sign also indicates the spin alignment for the atoms, where $J < 0$ corresponds to ferromagnetic

coupling and $J > 0$ to antiferromagnetic coupling.

$\hat{\mathbf{S}}_i = (\hat{S}_x \ \hat{S}_y \ \hat{S}_z)^T$ is the spin operator of atom i in the total system, which is defined for N atoms as:

$$\mathbf{S}_i = \mathbb{I}_1 \otimes \cdots \otimes \mathbb{I}_{i-1} \otimes \boldsymbol{\sigma}_i \otimes \mathbb{I}_{i+1} \otimes \cdots \otimes \mathbb{I}_N. \quad (2.2)$$

This operator consists of N Kronecker products and it only applies $\boldsymbol{\sigma}$, the single atom spin operator, on the i^{th} atom and applies identity on the other atoms. For spin- S system the single atom spin operator $\boldsymbol{\sigma}$ is a square matrix of dimensions $(2S + 1)$ with states $|S, m\rangle$ ($m = -S, \dots, S$ in integer steps) and satisfies the selection rules:

$$\begin{aligned} \langle m' | \hat{S}_x | m \rangle &= (\delta_{m', m+1} + \delta_{m'+1, m}) \frac{1}{2} \sqrt{S(S+1) - m'm}. \\ \langle m' | \hat{S}_y | m \rangle &= (\delta_{m', m+1} - \delta_{m'+1, m}) \frac{1}{2i} \sqrt{S(S+1) - m'm}. \\ \langle m' | \hat{S}_z | m \rangle &= \delta_{m', m} m. \\ \langle m' | \hat{S}_+ | m \rangle &= \delta_{m', m+1} \sqrt{S(S+1) - m'm}. \\ \langle m' | \hat{S}_- | m \rangle &= \delta_{m'+1, m} \sqrt{S(S+1) - m'm}. \\ \langle m' | \hat{\mathbf{S}}^2 | m \rangle &= \delta_{m', m} S(S+1). \end{aligned} \quad (2.3)$$

The single spin operator for a spin-1/2 system are the Pauli spin matrices:

$$\sigma_x, \sigma_y, \sigma_z = \begin{pmatrix} 0 & 1 \\ 1 & 0 \end{pmatrix}, \begin{pmatrix} 0 & i \\ -i & 0 \end{pmatrix}, \begin{pmatrix} 1 & 0 \\ 0 & -1 \end{pmatrix}. \quad (2.4)$$

Single spin operator for a spin-2 system is:

$$\begin{aligned} \sigma_x, \sigma_y, \sigma_z &= \frac{1}{2} \begin{pmatrix} 0 & 2 & 0 & 0 & 0 \\ 2 & 0 & \sqrt{6} & 0 & 0 \\ 0 & \sqrt{6} & 0 & \sqrt{6} & 0 \\ 0 & 0 & \sqrt{6} & 0 & 2 \\ 0 & 0 & 0 & 2 & 0 \end{pmatrix}, \frac{1}{2i} \begin{pmatrix} 0 & 2 & 0 & 0 & 0 \\ -2 & 0 & \sqrt{6} & 0 & 0 \\ 0 & -\sqrt{6} & 0 & \sqrt{6} & 0 \\ 0 & 0 & -\sqrt{6} & 0 & 2 \\ 0 & 0 & 0 & -2 & 0 \end{pmatrix}, \\ &\begin{pmatrix} 2 & 0 & 0 & 0 & 0 \\ 0 & 1 & 0 & 0 & 0 \\ 0 & 0 & 0 & 0 & 0 \\ 0 & 0 & 0 & -1 & 0 \\ 0 & 0 & 0 & 0 & -2 \end{pmatrix}. \end{aligned} \quad (2.5)$$

From the definition it can be seen that generally $\hat{\mathbf{S}}_i$ operates on a $(2S + 1)^N$ dimensional complex vector space, where S is the spin of the system e.g. spin-1/2 system consisting of two atoms would result in a total spin operator $\hat{\mathbf{S}}_i$ operating on a 4 dimensional complex vector space.

2.1.2 Anisotropy and Zeeman Hamiltonian

Atoms consist of a nucleus and an electron cloud, where the nucleus contains protons and neutrons and the electron cloud contains electrons. The protons of the atom attract the electrons, this creates a potential well where each electron forms a standing wave. The wave is best described by atomic orbitals, which is a mathematical function that contains the probability of the electron's position in space.

Atoms on a crystalline surface experience a magnetic anisotropy, which is favoring of the magnetization in a certain direction. The crystal field breaks the symmetry of the outer shell atomic orbitals, making the orbitals along the crystalline axes more favourable. The anisotropy of the orbitals is then carried over to the intrinsic spin, due to spin-orbit coupling. The electrons however, will still occupy the orbitals according to Hund's rules and depending on which orbitals are half filled will determine the magnetization.

The effect of an external magnetic field can be described by the Zeeman effect and the Hamiltonian that corresponds to this and the crystal field is [1]:

$$\hat{H}_{Ani} = \sum_{i=1}^N -g\mu_B \mathbf{B}_i \cdot \hat{\mathbf{S}}_i + D\hat{S}_{z,i}^2 + E(\hat{S}_{x,i}^2 - \hat{S}_{y,i}^2). \quad (2.6)$$

Where the first term is the Zeeman effect and the second and third term correspond to the magnetic anisotropy. g is the g-factor, μ_B is Bohr magneton, \mathbf{B}_i is the magnetic field on atom i and $\hat{\mathbf{S}}_i = (\hat{S}_x \ \hat{S}_y \ \hat{S}_z)^T$ is the spin operator for atom i of the total system defined as (2.2). $D = -\frac{\lambda^2}{2}(2\Lambda_{zz} - \Lambda_{xx} - \Lambda_{yy})$ and $E = -\frac{\lambda^2}{2}(\Lambda_{xx} - \Lambda_{yy})$ are the uniaxial and transverse magnetic anisotropy parameters respectively, λ is the spin-orbit coupling and Λ_{ii} are the components of the anisotropy tensor.

The magnitude of Λ_{ii} represents the geometrical symmetry of the surrounding e.g. $\Lambda_{xx} = \Lambda_{yy} = \Lambda_{zz}$ corresponds to an isotropic system and $\Lambda_{xx} = \Lambda_{yy} \neq \Lambda_{zz}$ corresponds to an uniaxial system. The largest magnitude of Λ_{ii} determines in which direction the magnetization aligns, this is called the easy-axis and by convention will correspond to the z-projection of the magnetization. In other words Equation (2.6) satisfies maximizing $|D|$ and $E > 0$.

D and E are phenomenological parameters commonly introduced, because they can be easier to understand. They share the same units as energy, while Λ_{ii} has the same units as the inverse of energy. D and E work well in a uniaxial system, where there is a clear easy-axis. D represents the splitting of the degenerate spin states $|m\rangle$ in the z-projection, while E mixes the states with different $|m\rangle$.

2.2 Analysis of Eigenvectors

Diagonalizing the Hamiltonian results in multiple eigenstates and corresponding eigenvalues. These eigenstates operate on the complex vector space $(\mathbb{C}^{2S+1})^{\otimes N}$, where S is the spin of the individual atoms and N is the number of atoms. The eigenstates of the Hamiltonian correspond to the whole system and on its own does not provide much insight to what the system is doing, specifically what the individual atoms are doing e.g. in an antiferromagnetically coupled spin chain. The eigenstates of the individual atoms $|\psi_i\rangle$ can be obtained by extracting them from the eigenstates of the whole system. A method to extract $|\psi_i\rangle$ is by calculating the expected value of an individual atom to be in one of the basis states and repeating this for all basis states and atoms. The eigenstates of the individual atoms $|\psi_i\rangle$ will be projected on the spin basis states corresponding to σ_z , these are for a spin-2 system:

$$|b_1\rangle = \begin{bmatrix} 1 \\ 0 \\ 0 \\ 0 \\ 0 \end{bmatrix}, |b_2\rangle = \begin{bmatrix} 0 \\ 1 \\ 0 \\ 0 \\ 0 \end{bmatrix}, |b_3\rangle = \begin{bmatrix} 0 \\ 0 \\ 1 \\ 0 \\ 0 \end{bmatrix}, |b_4\rangle = \begin{bmatrix} 0 \\ 0 \\ 0 \\ 1 \\ 0 \end{bmatrix}, |b_5\rangle = \begin{bmatrix} 0 \\ 0 \\ 0 \\ 0 \\ 1 \end{bmatrix}. \quad (2.7)$$

A basis state for the whole system consisting of N atoms is defined as:

$$|b_k\rangle_i = \mathbb{I}_1 \otimes \cdots \otimes \mathbb{I}_{i-1} \otimes |b_k\rangle \otimes \mathbb{I}_{i+1} \otimes \cdots \otimes \mathbb{I}_N, \quad (2.8)$$

where \mathbb{I} is identity matrix and $|b_k\rangle_i$ is the basis state k applied on atom i .

The probability of a individual atom to be in a basis state can be calculated as:

$$|\langle \psi_i | b_k \rangle|^2 = \langle \Psi | (|b_k\rangle_i) \cdot (\langle b_k |_i) | \Psi \rangle, \quad (2.9)$$

where $|\Psi\rangle$ is an eigenstate of the whole system.

Another method when working with statistical ensembles, in other words ensembles of eigenstates of the whole system, is the partial trace. The partial trace uses the basis states to trace the density operator corresponding to a specific eigenstate of the whole system. The result is a density operator which corresponds to the system with the atoms that were not traced.

The probabilities of the i^{th} atom in the basis states can be found by partial tracing all the other atoms from the total density operator and then trace the individual atom density operator with respect to the basis states.

The general density operator is defined as follows:

$$\hat{\rho} = \sum_k p_k |\phi_k\rangle \langle \phi_k|. \quad (2.10)$$

Where p_k is the probability to be in state $|\phi_k\rangle$.

Taking a single partial trace with respect to the last (N^{th}) atom $\text{Tr}_N(\rho_{\text{total}})$ looks as follows:

$$\rho_{1,\dots,N-1} = \text{Tr}_N(\rho_{\text{total}}) = \sum_{k=1} (\langle b_k|_N \cdot \rho_{\text{total}} \cdot |b_k\rangle_N). \quad (2.11)$$

where the summation covers all the basis states and $\rho_{\text{total}} = \rho_{1,\dots,N}$ is the density matrix of the whole system for a specific eigenstate.

Finding the density matrix for a single atom n :

$$\rho_i = \sum_k p_k |b_k\rangle \langle b_k| = \text{Tr}_{1,\dots,i-1,i+1,\dots,N}(\rho_{\text{total}}), \quad (2.12)$$

The probabilities can be found by tracing the single atom density matrix with respect to spin basis states:

$$\begin{aligned} |\langle \psi_i | b_k \rangle|^2 = p_k &= \text{Tr} \left(\sum_j \langle b_k | b_j \rangle p_j \langle b_j | b_k \rangle \right) && \text{(orthogonal)} \\ &= \text{Tr}(\langle b_k | \left[\sum_j p_j |b_j\rangle \langle b_j| \right] |b_k\rangle) && (2.13) \\ &= \text{Tr}(\langle b_k | \rho_i | b_k \rangle) && \text{(cyclic property)} \\ &= \text{Tr}(\rho_i |b_k\rangle \langle b_k|). \end{aligned}$$

To give an example for how the partial trace looks like, consider $S = 2$, $N = 3$ and the density matrix of the second atom needs to be recovered:

$$\begin{aligned} \rho_2 &= \text{Tr}_{1,3}(\rho_{1,2,3}) = \text{Tr}_1(\text{Tr}_3(\rho_{1,2,3})) \\ &= \text{Tr}_1 \left(\sum_k (\mathbb{I}_1 \otimes \mathbb{I}_2 \otimes \langle b_k |) \cdot \rho_{1,2,3} \cdot (\mathbb{I}_1 \otimes \mathbb{I}_2 \otimes |b_k\rangle) \right) \\ &= \sum_k (\langle b_k | \otimes \mathbb{I}_2) \cdot (\rho_{1,2}) \cdot (|b_k\rangle \otimes \mathbb{I}_2). \end{aligned}$$

The probabilities of $|\psi_i\rangle$ in the basis states can be extracted with (2.13)

2.3 Frustrated systems

Intrinsic magnetic frustration refers to a conflict in minimizing exchange interaction energy. This occurs when it is impossible to satisfy all exchange interaction between spin pairs and allows the system to arrange in many equivalent minimum-energy configurations [11], leading to massive intrinsic degeneracy of the ground state.

A simple system containing frustration is the antiferromagnetically coupled Ising model on a triangle. The three spins cannot all be anti-parallel to each other and results in a frustrated system. Figure 2.1 shows the six-fold degenerate ground state of the triangle.

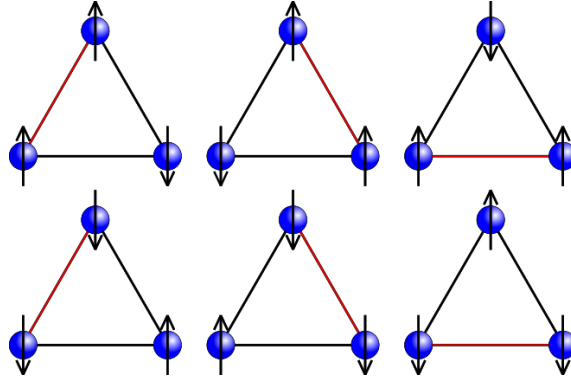


Figure 2.1: The six possible ground states of the antiferromagnetic Ising model on an equilateral triangle. The red line indicates the frustrated ferromagnetic coupled pair.

The underlying lattice for this Ising triangle needs to be hexagonal and has been done on pt (111) [8]; However, the adatoms were placed directly on bare metal. This thesis makes use of a square lattice, which has an insulating layer and large magnetic anisotropy, resulting in better spin distinction. It is not possible to build the equilateral frustrated system on this sample; Therefore, a different structure is required.

The square lattice used for the experiment is $\text{Cu}_3\text{Au}(100) - c(2 \times 2)\text{N}$ and is similar to Cu_2N [12]. The coordinate system that is adopted throughout the thesis is, with respect to the position of the atom, defined as: the z-axis along the nitrogen direction, the x-axis along the hollow direction and the y-axis is out of plane, shown in Figure 2.2a.

Magnetic atoms spin-couple with each other on Cu_2N , when placed at a close distance. This coupling originates from indirect interaction between spins that is mediated by non magnetic nitrogen atoms, known as superexchange interaction [13], and/or by the conduction electrons of the underlying metal, known as RKKY interaction [14]. Depending on the coupling between the atoms (antiferromagnetic and ferromagnetic), it is possible to build a structure that has a frustrated ground state. For iron on Cu_2N , the coupling for vertically and horizontally placed iron atoms is antiferromagnetic, and diagonally placed Fe atoms is ferromagnetic [10] shown in Figure 2.2b. In the Figure the atoms coupled with J_1 are interacting through superexchange and RKKY, while J_2 only has RKKY. This results in J_1 and J_2 having different magnitudes even though the distance between atoms are the same. The

schematics throughout this thesis have the Cu_2N lattice removed in order to simplify them, seen in Figure 2.2c

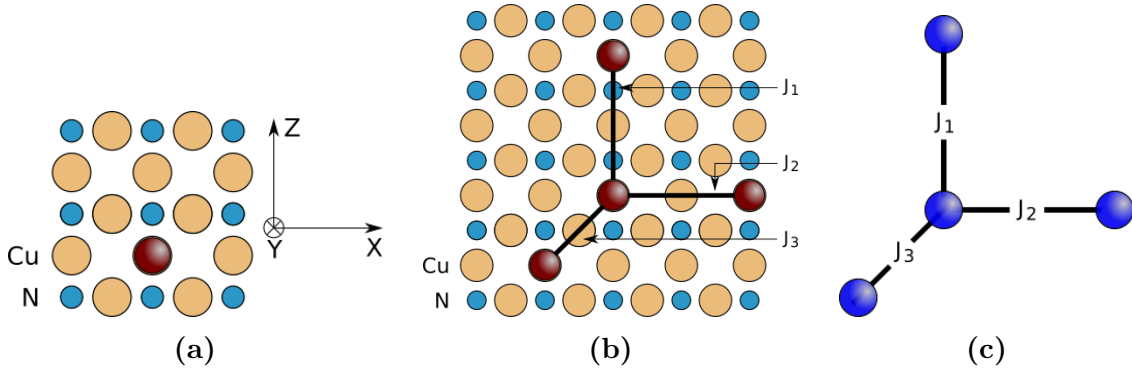


Figure 2.2: **(a)** Schematic of Cu_2N lattice, where Cu is the bigger yellow circle and N is the smaller blue circle. The coordinate system is determined with respect to the adatom (red sphere), z is along N-direction, x is along hollow-direction and y is out-of-plane direction. Figure adapted from [1]. **(b)** The different couplings between adatoms according to the angle and distance between them. J_1 is along the N direction and is antiferromagnetic, J_2 is along the hollow direction is antiferromagnetic but weaker than J_1 and J_3 is ferromagnetic. **(c)** The different couplings, but now the Cu_2N background is removed for simplification.

The smallest configuration for a frustrated system on a square lattice for iron is shown in Figure 2.3.

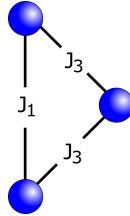


Figure 2.3: The smallest frustrated system on a square lattice, where J_1 is antiferromagnetic and J_3 is ferromagnetic, and $|J_1| \approx |J_3|$.

In this configuration however, the atoms are so close to each other, that it is difficult to assemble such a structure. An easier configuration with respect to building is a ‘D’ structure (it looks like a letter D), which is shown together with an intrinsic frustrated state in Figure 2.4.

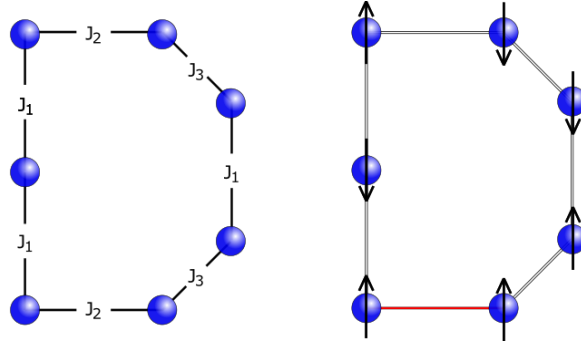


Figure 2.4: The ‘D’ structure, where J_1 , J_2 are antiferromagnetic and J_3 is ferromagnetic, and $|J_1| \approx |J_3|$, $|J_2| < |J_1|$. In the right panel an example of one of the 4 degenerate ground states, the frustration is indicated in red.

2.4 IETS: Inelastic Electron Tunneling Spectroscopy

Inelastic electron tunneling spectroscopy in a scanning tunneling microscope (STM) is a technique to measure spin excitation of a single atom on a crystalline surface. This technique can be used to distinguish atoms on a surface that have a unique splitting and filling of the orbitals, which will give a corresponding unique spectrum.

Quantum tunneling is a physical phenomenon where it is possible for particles to overcome potential barriers, which they classically could not. In an STM the electrons tunnel through the vacuum between tip and sample and therefore creating a tunnel current, I_t . The electrons can tunnel elastically or inelastically. In the first case the electrons do not lose energy in the process. In the second case the electrons lose energy, which can be absorbed by the sample resulting in a magnetic excitation. This excitation can only occur when the applied bias voltage, V_b , between tip and sample is larger than the excitation energy ($eV > \Delta E$).

In Figure 2.5 the process of tunneling is shown. First the adatom is in the ground state, then a spin down electron tunnels from the tip to the adatom and finally an electron tunnels from the adatom to the sample. If the outgoing electron has the same spin as the incoming electron, then the adatom is in the ground state and the magnetization stays the same, and this is elastic tunneling. The other case is inelastic tunneling, where the spin of the outgoing is different from the incoming electron, the adatom is then in an excited state and the magnetization of the adatom has changed.

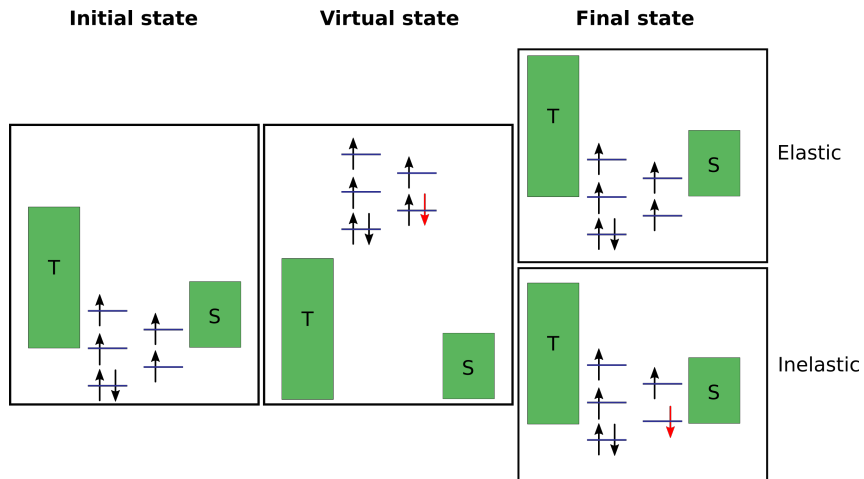


Figure 2.5: General process of tunneling in an STM. The adatom starts in the ground state, an electron tunnels through the barrier putting the adatom in a virtual state and finally the adatom relaxes to the ground state (elastic tunneling) or excited state (inelastic tunneling). In the inelastic tunneling case the magnetization has changed. Image adapted from reference [1]

Chapter 3

Numerical simulation methods

This chapter will cover the technicalities of implementing the models in section 3.1 and the probabilities of the individual atoms with respect to the basis states in section 3.2.

3.1 The Hamiltonian

The Heisenberg Hamiltonian as defined in Equation (2.1) is suited for quasi-one dimensional magnetic systems e.g. spin chains. A more general expression would be to have spin interaction between all the atoms and have J depend on the distance and angle between them. atoms that are far apart have $J = 0$ and in the case of a uniaxial system there is a difference in strength if the atoms are coupled along the easy axis or along the hard axis with respect to the surface, seen in Figure 2.2b. In order to prevent counting terms double due to symmetry, the second sum in the Heisenberg Hamiltonian only goes up to index i .

The total Hamiltonian consist of three parts, where the Heisenberg Hamiltonian is now expressed for 2D magnetic structures:

$$\begin{aligned}\hat{H}_{Heis} &= \sum_{i=1}^N \sum_{j=1}^i J_{ij} \hat{\mathbf{S}}_i \cdot \hat{\mathbf{S}}_j. \\ \hat{H}_{Ani} &= \sum_{i=1}^N D_i \hat{S}_{z,i}^2 + E_i (\hat{S}_{x,i}^2 - \hat{S}_{y,i}^2). \\ \hat{H}_{Zee} &= \sum_{i=1}^N -g\mu_B \mathbf{B}_i \cdot \hat{\mathbf{S}}_i.\end{aligned}\tag{3.1}$$

g , μ_B are constants and only have to be declared once. D_i , E_i , \mathbf{B}_i are arrays containing the corresponding value for atom i .

The spin operator \hat{S}_i for N atoms is defined as Equation (2.2), it consists of N terms which interact with each other through the Kronecker product. The index i indicates which atom is affected by the single spin operator. The single spin operator is obtained by the selection rules in Equation (2.3) and depends on the spin of the single atom.

The big difference, when implementing the Hamiltonian, between a quasi-one dimensional chain and a 2 dimensional structure is the number of couplings a single atom can have. The quasi-one dimensional case only takes into account nearest neighbours, as a result in one dimension the number of couplings a single atom can have is at most two and since the coupling between A and B is the same as B and A, the amount of J 's scale with N , shown in Figure 3.1a. This makes keeping track of the J 's predictable and it can be declared in a single array and positions of the atoms do not have to be specified. In 2 dimensions the amount of couplings a single atom can have varies from 1 to N , therefore creating a single array of J values can become incomprehensible e.g. in Figure 3.1b the middle atom has 4 couplings. This calls for a code that determines the J values between atoms depending on the distance and orientation. In order to make this work the positions of the atoms need to be specified and the J 's need to be defined corresponding to a specific distance and angle e.g. atoms with a lattice distance of 2 have a stronger J than atoms with a lattice distance of 3.

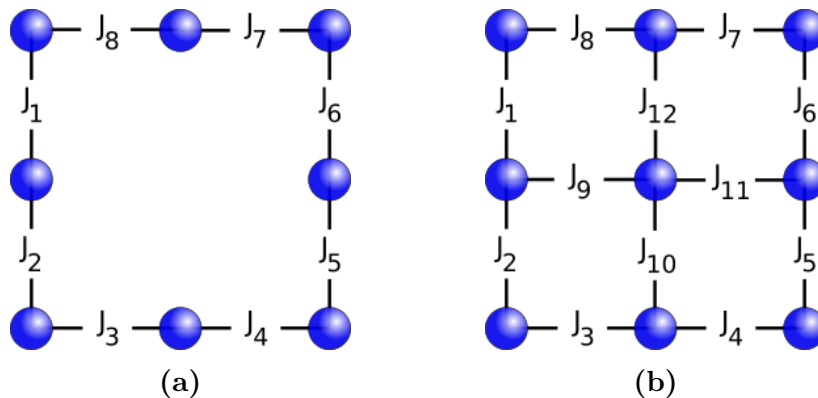


Figure 3.1: The number of coupling terms that need to be taken into account differs for a quasi-one dimensional system (a) and a two dimensional system (b). In (a) the number of coupling terms won't exceed the number of atoms. In (b) a single atom can have more than two couplings and thus the amount of coupling terms can be quite large making book keeping difficult.

A problem with quantum systems is the size of the Hamiltonian, since it increases exponentially with the number of atoms and as a result it takes up a lot of memory. To reduce memory usage the Hamiltonian matrix is made sparse, this means that only the nonzero elements are stored in memory instead of all the matrix el-

ements. To put things into perspective the Hamiltonian for a spin system has a size of $(2S + 1)^N \times (2S + 1)^N$. For a spin chain consisting of 6 Fe atoms ($S = 2$, $N = 6$) gives $2.4 \cdot 10^8$ complex matrix elements and is stored as two double-precision floating-points. The memory usage of the 6 atom chain takes up ~ 4 GB and increasing it to 7 atoms takes ~ 100 GB. Since the spin operators consist of Kronecker products with identity operator, the Hamiltonian matrix contains a lot of zero's and would benefit from being sparse. Now for the sparse 7 atom Hamiltonian it only takes ~ 200 MB of memory.

The total Hamiltonian is obtained by summing the three parts ($\hat{H}_{Total} = \hat{H}_{Heis} + \hat{H}_{Ani} + \hat{H}_{Zee}$) and the eigenenergies and eigenstates are obtained by diagonalizing the resulting Hamiltonian. Since the Hamiltonian is a sparse matrix the diagonalization is done with the Lanczos algorithm. The algorithm finds k most useful eigenvalues and eigenvectors for a $n \times n$ Hermitian matrix, where $k < n - 2$.

3.2 Expectation values

The probabilities can now be obtained by calculating the expected value of an operator that operates on atom n with respect to the single atom basis states. The operator will be defined as a matrix multiplication of Equation (2.8) and the matrix has a size of $(2S + 1)^N \times (2S + 1)^N$:

$$M_{n,i} = (\mathbb{I}_1 \otimes \cdots \otimes \mathbb{I}_{n-1} \otimes |b_i\rangle \otimes \mathbb{I}_{n+1} \otimes \cdots \otimes \mathbb{I}_N) \\ \cdot (\mathbb{I}_1 \otimes \cdots \otimes \mathbb{I}_{n-1} \otimes \langle b_i| \otimes \mathbb{I}_{n+1} \otimes \cdots \otimes \mathbb{I}_N).$$

The expected value is taken by sandwiching the operator with eigenstates of the whole system as in Equation (2.9):

$$|\langle \psi_n | b_i \rangle|^2 = \langle \Psi | M_{n,i} | \Psi \rangle.$$

Finally this will be repeated for all basis states and for each individual atom.

Chapter 4

Experimental methods

This chapter will cover the methods used for the experiment. Section 4.1 provides a general description of the STM, the sample preparation and the measuring techniques available. This is followed by a description of single atom manipulation in section 4.2.

4.1 Scanning tunneling microscope

Scanning probe microscopy, SPM, is a branch of microscopy, which does not use light to form images. Instead it uses a physical probe to scan the sample. SPM started with the invention of the STM in 1981 by Rohrer and Binnig [15], where they successfully imaged surfaces with atomic precision [16]. Since then other forms of SPM have emerged e.g. Atomic force microscopy [17]. The research for this thesis was done in an STM, which was readily available in the Ottelab group.

The STM is an instrument that scans over a surface using a sharp needle, also known as the STM tip, and is able to resolve features at the atomic scale. An image is made by applying a bias voltage, V_b , between STM tip and sample, and recording the resulting tunnel current at each point. The sensitivity of the STM for atomic scale features also means that it is susceptible to contamination (other unwanted atoms/molecules). In order to reduce the contamination the experiments and sample preparations are done in Ultra High Vacuum (UHV, $P < 10^{-10}$ mbar). Another property of the STM used in this thesis are the very low temperatures (< 1 K), this disables atomic motion and opens up the possibility to study electron spin excitation (of the order of a few meV).

4.1.1 Unisoku USM1300

The STM used for the experiments is a USM 1300-3He system by Unisoku. It is a low-temperature ultra-high-vacuum system, shown in Figure 4.1a. The low temperatures are achieved by using liquid ^4He and ^3He and gives the system two operational

temperatures, these are for the sample 1.5 K and 350 mK. The first temperature is reached by Joule-Thomson cooling liquid ^4He , which decreases the temperature to ~ 1 K. The second is reached by condensing ^3He and has a holding time of ~ 28 hours. The pressure of the STM chamber is of the order of 10^{-10} mbar, which is achieved by a series of pumps. This STM is also equipped with superconducting magnets consisting of a solenoid, which can generate a magnetic field up to 9 T perpendicular to the surface of the sample, and a split-coil generating up to 2 T in one axis parallel to the surface.

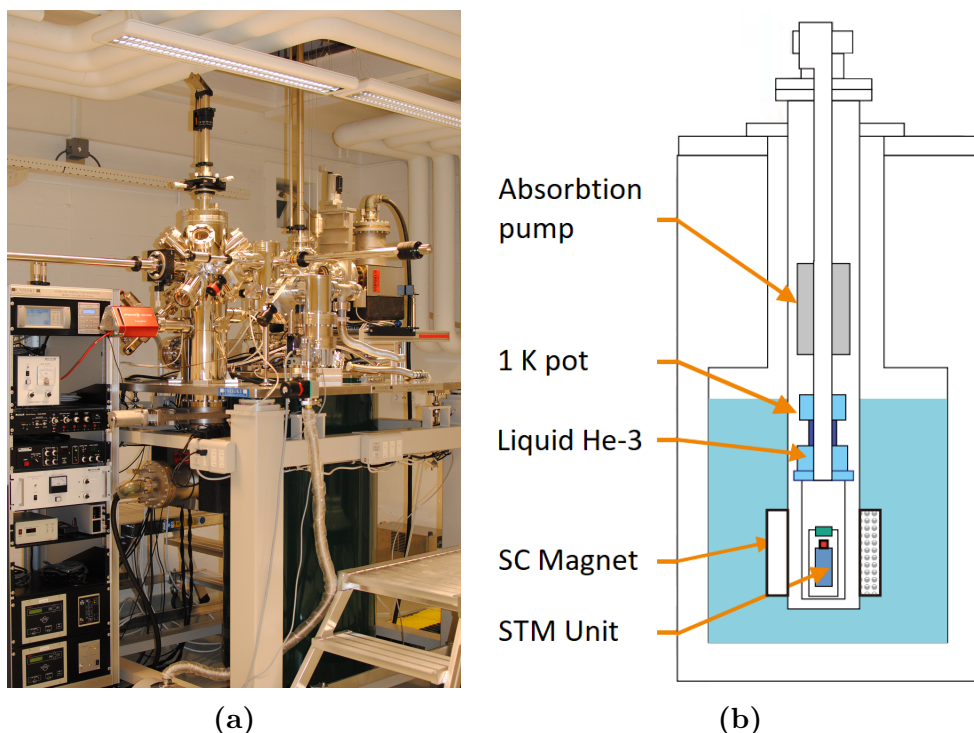


Figure 4.1: **(a)** A picture of the Unisoku UMS 1300. The system is on top of a floating table in order to reduce vibrations, where the three vacuum chambers on top of the table and the green cryostat (also floating) is under the table. **(b)** Schematic of the cryostat from the STM. The absorption pump is for condensing ^3He , the 1 K pot houses the ^4He , the SC Magnet is used to create an external field and the STM unit houses the STM-tip and sample. The image was taken from the Unisoku UMS 1300 website.

The STM consists of four main parts: The cryostat, the exchange chamber, the preparation chamber and the load lock, of which the last three and the insert of the cryostat are in vacuum. The cryostat, shown in Figure 4.1b houses the STM tip, the superconducting magnets and the liquid helium; This is also where the measurements are done.

The exchange chamber, situated above the cryostat, has evaporators installed and are used to evaporate metals onto the surface of the sample. The sample descends from the exchange chamber into the cryostat via a transfer bar.

The preparation chamber, connected to the exchange chamber, is where the sample gets prepared. It contains an ion gun for sputtering, a sample e-beam and a tip e-beam for annealing, and a LEED (low-energy electron diffraction) system to view the crystalline structure and composition of the surface.

The load lock, connected to the preparation chamber, is where samples and tips are loaded into the system. The chamber is easily isolated from the rest of the system and can be opened to the outside world. After the load lock has been opened it first needs to be pumped to UHV pressure, before transferring the sample and tips further into the system.

4.1.2 Sample preparation of Cu_3AuN_2

Over the past few decades thin insulating layers have played a major role in surface science [18, 19, 20]. An STM relies on the conductance of the adsorbates to form images and probe electronic properties and therefore conducting substrates are necessary. However having the adsorbates on the bare substrate causes the adsorbate electrons to be perturbed by the substrate electrons and hinders the study of electronic properties. The solution is a thin insulating layer of only a few atoms thick, it provides sufficient decoupling of the electrons and is still able to let a current flow.

A suitable sample for building atomic structures is the combination of nitrogen and Cu(100) crystal. providing self assembly of insulating nitrogen islands [21], which decouples the spin of the adatom from the conduction electrons of the surface. It also provides a large uniaxial anisotropy [22] allowing for tunable spin-spin coupling between neighbouring atoms. The sizes of the atomic structures are only limited by the size of the nitrogen islands. For Cu_2N the island sizes are strain limited to $\sim 5 \times 5 \text{ nm}^2$ [23]. Due to a mismatch between the lattice constant of Cu_2N and bare Cu(100), which are $a_{\text{Cu}_2\text{N}} \approx 3.72 \text{ \AA}$ and $a_{\text{Cu}_2\text{N}} \approx 3.6 \text{ \AA}$ respectively. To overcome the growth limitation, a crystal substrate with a lattice constant that better matches $a_{\text{Cu}_2\text{N}}$ is required. This thesis uses the crystal $\text{Cu}_3\text{Au}(100)$, which has a lattice constant of $a_{\text{Cu}_3\text{AuN}} \approx 3.75 \text{ \AA}$ [24] and forms large continuous insulating islands reaching 100 nm [12]. The manipulation of atoms on this surface will be discussed in section 4.2

Sample preparation is mostly done in the preparation chamber and starts of with cleaning the metallic crystal, in this case $\text{Cu}_3\text{Au}(100)$, by means of multiple rounds of sputtering and annealing.

Sputtering is a process where high energy ions are shot at the metal to clean it. For cleaning purposes the element Ar is used, the Ar atoms are let into the preparation chamber and they are electrically neutral. With an ion gun the Ar is ionized and with a high voltage potential they are accelerated towards the sample. This removes the surface and gets rid of potential contamination.

Annealing is a process where the metal is heated in order to flatten the surface and bring impurities to the surface. The sample is heated by the accelerated electrons coming from the filament when a bias voltage is applied. The heat softens the metal, which make it possible for atoms to migrate and decrease the amount of dislocations and internal stresses pushing impurities to the surface.

After the metal is cleaned, seen in Figure 4.2a, the insulating layer is grown and more specifically $\text{Cu}_3\text{Au}(100) - c(2 \times 2)\text{N}$ (will be denoted as Cu_3AuN_2). The N_2 gets sputtered on the Cu_3Au , similar to Ar sputtering, and then the whole sample is annealed. This forms a one atom thick layer of Cu_3AuN_2 islands, seen in Figure 4.2b with an average size of 30 nm x 30 nm.

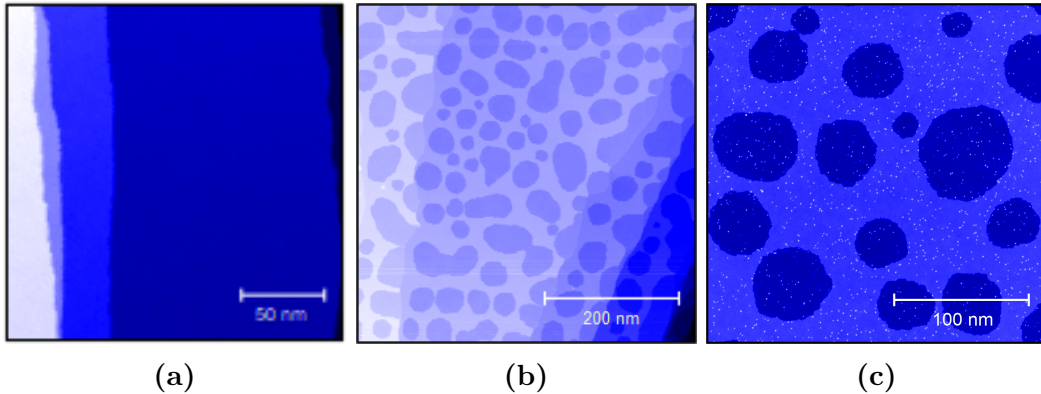


Figure 4.2: Topography images of the three sample preparation stages: **(a)** clean $\text{Cu}_3\text{Au}(100)$ after annealing and sputtering, **(b)** insulating N islands on $\text{Cu}_3\text{Au}(100)$ and **(c)** Evaporated Fe atoms on $\text{Cu}_3\text{Au}(100) - c(2 \times 2)\text{N}$. The nitrogen islands, visible in **(b)** and **(c)**, are the darker patches surrounded by the brighter area and the Fe atoms are the white dots in **(c)**. The images were taken at 1 K, **(a)** 500 pA and 300 mV, **(b)** 20pA and 100 mV and **(c)** 20 pA and 50 mV.

Finally the magnetic atoms are evaporated on the surface, for this experiment Fe is used. Ideally the evaporation should be done in the cryostat to keep the temperature of the sample low and therefore preventing clustering of the Fe atoms. In this STM however the sample faces downwards and below the sample is the STM tip, which prevents evaporation in the cryostat. For this reason the evaporation is done in the exchange chamber, minimizing the time spent at room temperature. Getting the

Fe atoms on the surface is done by heating an Fe rod near its melting point, this evaporates a part of it creating a flow of Fe atoms. The sample, which is already cold, is then moved into the flow and kept there for a few seconds to get enough Fe on the sample. The resulting sample with evaporated Fe is shown in Figure 4.2c

4.1.3 Topography

STM Topography is a method of visualizing the surface and what lies on it, using a tip to make a scan. The STM tip is a sharp needle situated a few 100 pm above the surface, which is so close that electrons can tunnel between tip and sample. If a bias voltage, V_b , is applied between them, a tunnel current I_t will flow. The magnitude of I_t is affected by the properties of the material, mainly if it is insulating (lower I_t) or conducting (higher I_t). To get a topography of the surface at a given V_b , the tip will scan the surface line by line and for every line, split up in discrete points, the magnitude of I_t will be displayed, keeping the tip height and V_b constant. The problem however with keeping the tip height constant is the possibility of crashing the tip into the surface, due to large molecules or steps in the crystal. A safer way is using “constant current mode”, a schematic of both scanning modes is shown in Figure 4.3. In constant current mode I_t is kept constant instead of tip height. As the tip crosses the surface, the STM will vary the tip height with a feedback loop in order to keep I_t constant. By tracking the tip height a topographic image can be made, shown in Figure 4.2.

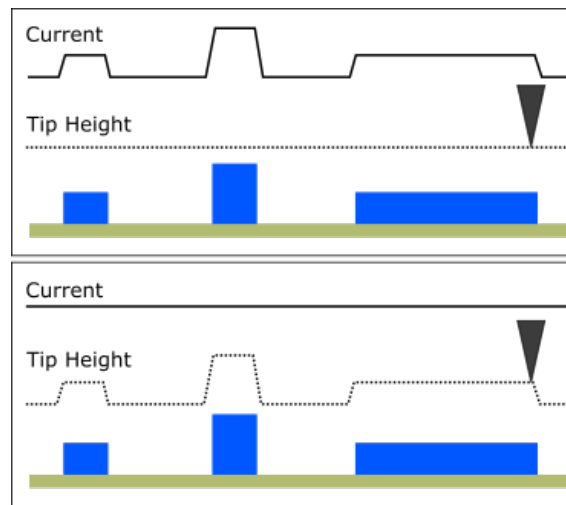


Figure 4.3: Schematics of the two scanning modes, the top panel shows constant height mode and the bottom panel shows constant current mode.

4.1.4 Spectroscopy

STM-IETS is a method to study spin excitations of an adatom and a detailed description can be found in section 2.4. The $I(V)$ curve from an STM can be obtained

in the following way: park the tip at a given position, turn off feedback to keep the tip height constant, sweep V_b over the relevant energy range and finally record the corresponding $I_t(V)$. An evaporated atom on a crystalline surface will have its spin states split, due to the crystal field and spin orbit coupling. When the STM tip is placed above such an adatom and if V_b is larger than the excitation energy of the atom ($eV > \Delta E$), then an excited state can be accessed for tunneling and will contribute to the conductance resulting in a slope change in the $I(V)$ curve. This change can be easily visualized in the differential conductance spectrum, which will look like a step. An example of a typical differential conductance spectrum for Fe on a Cu_2N surface is shown in Figure 4.4a, at zero V_b the excitation energy has not been reached and as the voltage increases steps appear and conductance increases. Another thing to note is the current going from tip to sample or from sample to tip does not affect the conductance, resulting in a symmetric differential conductance around $V_b = 0$.

The differential conductance dI/dV can be calculated numerically from the $I(V)$ curve, however this is prone to noise and can be avoided by using a lock-in-amplifier. The lock-in technique adds a sinusoidal wave (with amplitude V_{mod} and frequency $f_{\text{lock-in}} \approx 1\text{KHz}$) to DC V_b , by measuring the difference of the response resulting from the wave the $\Delta I/\Delta V$ can be acquired, as seen in Figure 4.4b, and for small enough V_{mod} this will correspond to dI/dV .

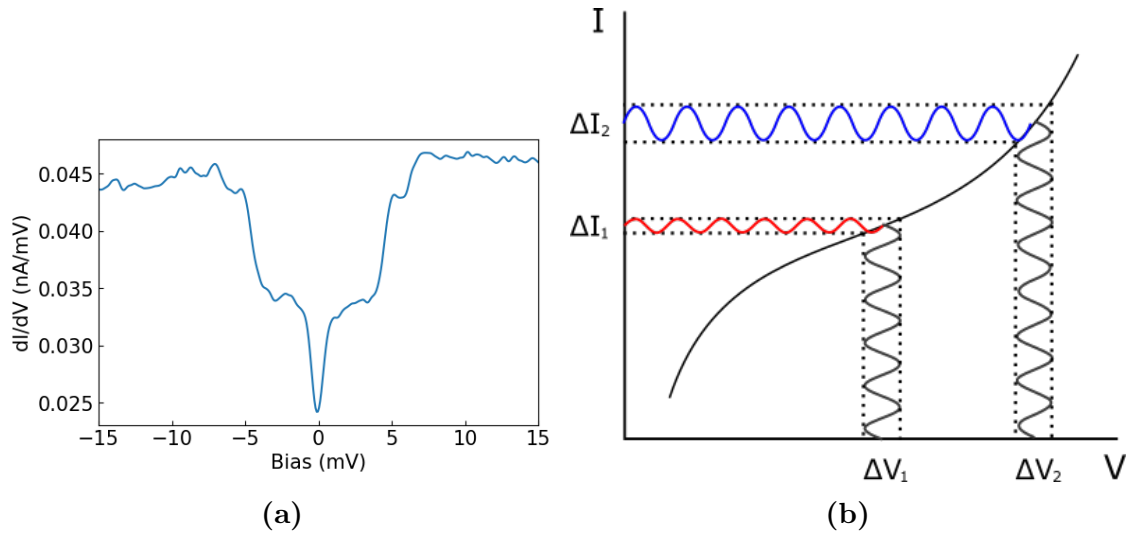


Figure 4.4: **(a)** The spectroscopy of a single Fe atom on Cu_3AuN_2 using the lock-in-amplifier taken at 330 mK and a setpoint of 20 mV and 1 nA. **(b)** Shows the way the lock-in-amplifier acquires the dI/dV , the amplitude of the incoming sine wave is determined by V_{mod} .

4.1.5 Spin-polarized STM

A tip is spin-polarized if it is able to resolve spin contrast, this spin sensitivity is achieved by having a magnetic atom on the apex of the tip. Spin-polarized STM (SP-STM) is a technique to study magnetism at the atomic scale by using a spin-polarized tip [25]. The Idea behind SP-STM is visualizing the polarization of the adatoms with the polarized tunneling electrons coming from the spin-polarized tip. The spin polarization of the tip can be determined by:

$$P = \frac{n_{\uparrow} - n_{\downarrow}}{n_{\uparrow} + n_{\downarrow}}, \quad (4.1)$$

where n_{\uparrow} and n_{\downarrow} are the density of states for the two states.

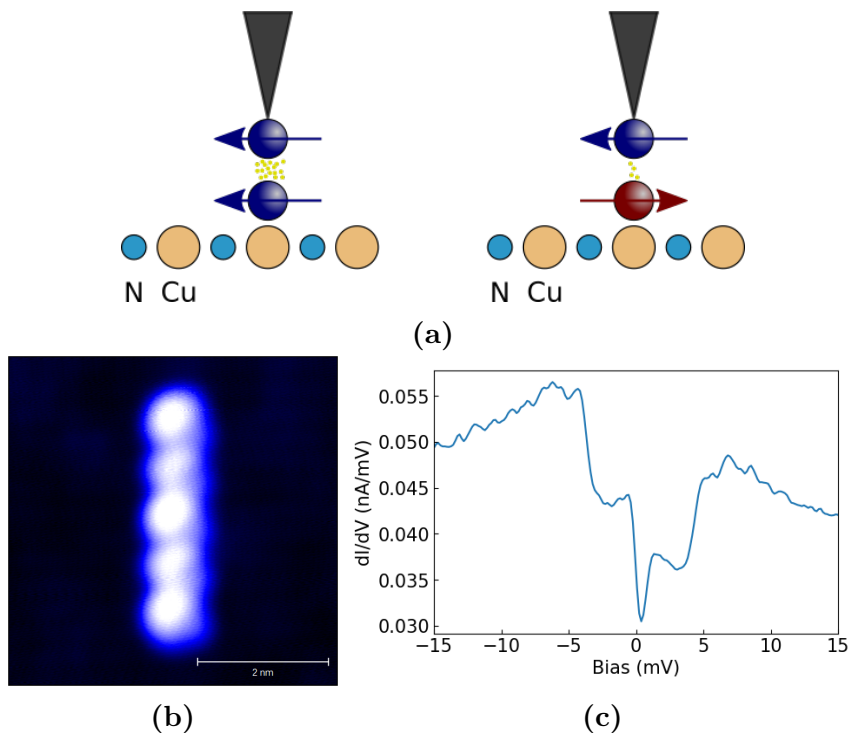


Figure 4.5: **(a)** Schematic of spin-polarized imaging. The tip has a single atom at the apex and the tunnel current will be higher or lower depending on the alignment of the adatom. Image adapted from [1]. **(b)** A topography of an antiferromagnetic structure made from Fe atoms on Cu_3AuN_2 taken with a spin-polarized tip at 50pA, 2 mV, 1 T and 330 mK. The difference in tunnel current is translated into a difference in size. The tip is polarized by applying a B -field along the easy-axis of Fe. **(c)** A Spectroscopy of a single Fe atom on Cu_3AuN_2 taken with a spin-polarized tip at 1 T, 330 mK and a setpoint of 1 nA and 1 T. The difference in tunnel current translates to the left half having a higher conductance than the right half.

The method used in this thesis to achieve a spin-polarized tip starts off with a non magnetic tip and picking up (vertical atom manipulation) magnetic atoms until a

single one is on the apex of it. When a magnetic field is applied, the magnetization of the magnetic atom on the tip will align in the direction of the magnetic field. As a result the magnitude of I_t will be different if the polarization of the apex atom and the adatom are parallel or anti-parallel, shown in Figure 4.5a. The effect on topography is shown in Figure 4.5b, in this case the larger (Circular) atom is associated with parallel polarization and the smaller (ellipsoid) atom is associated with anti parallel polarization. The effect on spectroscopy is shown in Figure 4.5c, where the left half has a higher conductance.

4.1.6 ESR: Electron spin resonance

With IETS an STM is able drive inelastic excitations of a spin system, revealing the energy excitations between levels. However the energy resolution of this method is limited by temperature, $\propto k_B T$, e.g. the energy resolution for the USM 1300-3He system at base temperature would be larger than $\sim 40 \mu\text{eV}$, which translates to a spectral resolution of $\sim 10 \text{ GHz}$. For reference a frustrated system as seen in Figure 2.4 has an energy splitting between ground state and first excited state in the order of $10^{-2} \mu\text{eV}$ (a few MHz) at 0.5 T along the nitrogen direction. This is 3 orders of magnitude smaller than the temperature-limited resolution.

In a recent experimental breakthrough by Baumann *et al.* [2] in 2015, where they demonstrate the combination of electron paramagnetic resonance with scanning tunneling microscope in order to measure the electron spin resonance of an individual Fe atom. Thereby reaching a higher spectral resolution than STM-IETS could. The experimental technique electron spin resonance (ESR) uses radio-frequency (RF) radiation to excite spin transitions. This gives it a high spectral resolution since the frequency needs to match the energy splitting precisely. Therefore, the combination of ESR with STM results in a better energy resolution at the same temperature.

ESR-STM is such a recent development that it has not been tested on surfaces other than MgO and therefore, also not on Cu_3AuN_2 . The Ottelab group is currently testing ESR-STM on this sample to verify the feasibility.

In general for an ESR experiment, the exact frequency needed to excite transitions is unknown, so the frequency has to be swept until the resonance frequency is met. It is also important to note, that reaching the resonance frequency is only one part to excite the system with RF. The other part is decided by the the selection rules, there needs to be a perturbing term that allows transitions between the states. In spin systems this is done by the \hat{S}_x and \hat{S}_y , which can be written in terms of ladder operators as $\hat{S}_x = \frac{1}{2} (\hat{S}_+ + \hat{S}_-)$ and $\hat{S}_y = \frac{1}{2i} (\hat{S}_+ - \hat{S}_-)$. Fe is a spin-2 system, on Cu_2N the spin states are split as Figure 4.6a, where the lowest energy states correspond to ± 2 . To excite the Fe atom from $+2$ to -2 with RF, the other spin states need to have a finite occupation.

ESR in STM works by measuring a difference in tunnel current on the resonant frequency on the spin, when RF is on and off. This difference is the result of population changes in ground state, P_0 , and excited state, P_1 , when RF resonance is on and off, which is shown in Figure 4.6b. The population changes are then made visible by SP-STM, because a spin polarized tip has a different magnitude of I_t depending on the population of the states. When RF resonance is off the spin population is distributed according to the Boltzmann distribution. When RF resonance is on, the spin population will change toward $P_0 = P_1 = 0.5$ [26].

It is important to be careful of other mechanism that are able to produce a tunneling current with RF dependence e.g. RF dependent power dissipation in the transmission lines. The transfer functions shows the RF voltage that arrives at the tunnel junction as a function of frequency. Once the transfer function has been determined for the system, the RF source power can be varied to reach a constant-amplitude frequency sweep.

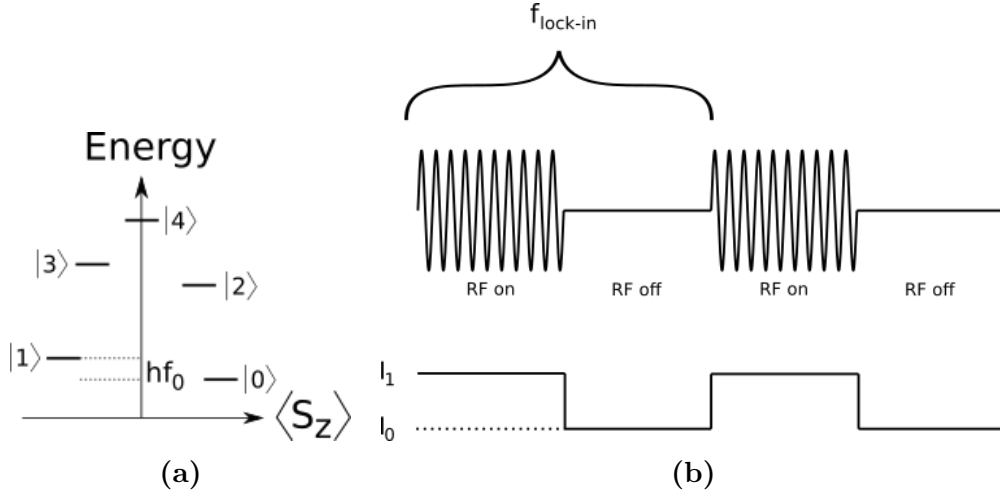


Figure 4.6: **(a)** Linear crystal field splitting on Fe, where a magnetic field B_z splits state $|0\rangle$ and $|1\rangle$. The image idea taken from reference [2]. **(b)** The RF chopping scheme for a lock-in measurement, the tunnel current is higher when RF is turned on.

4.2 Single atom manipulation

Single atom manipulation is made possible by precise control of the interaction between the atom of the STM-tip and the adatom. The STM-tip at imaging distance exerts a finite force on the sample directly below it. This distance for imaging is far enough to not disturb the probed atom, thus manipulation of the adatom can be achieved by moving the tip closer.

There are two distinct types of atom manipulation: lateral and vertical. In lateral manipulation the atoms are dragged along a flat metal surface [27], this is done by lowering the tip next to the adatom and adjusting the bias voltage in order to increase the tip-sample interaction. In vertical atom manipulation the atoms are picked up from the surface and dropped off in the desired position [20]. Also in this case the tip is lowered to increase the tip-adatom interaction, but now an electric field is applied to transfer the atom from the sample to the tip or vice versa.

The main advantage of using lateral manipulation is less impact on the tip and surface, which relaxes the stability threshold of the tip and the sample composition. This comes from the notion that dragging an atom along the surface should take less force than pulling it off the surface. However lateral manipulation is best suited for dense-packed surfaces and this is not the case in the studied sample, Cu_3AuN_2 , where the nitrogen forms a $c(2 \times 2)$ adlayer. Another reason is the evaporated Fe is bound strongly to the Cu_3AuN_2 , because the Fe forms two covalent bonds with the nitrogen (N-Fe-N). So this thesis will focus on vertical atom manipulation.

4.2.1 Vertical atom manipulation

The success of vertical atom manipulation depends highly on the shape and stability of the tip, and therefore preparation of the tip for manipulation is necessary. Tip preparation is done by pushing the tip a few nanometers into the metallic substrate, also known as a tip-crash, and applying a bias voltage (a few volts). The resulting thermal energy [28] reshapes the apex of the tip to be sharper and the tip will also be coated in the metal of the sample (in this case Cu_3Au). The tip-crash is repeated until manipulation is successful and stable. Important to note is that tip-crashing into the nitrogen is not desirable for manipulation, since it will put nitrogen on the tip. The picked up Fe will bind to the nitrogen and this will in turn make it very hard to drop the Fe atom.

The process of vertical atom manipulation can be explained by using a double potential well, shown in Figure 4.7. When the tip is within tunneling regime the atom has two stable positions, on the tip and on the surface. Each position is represented by a potential well and they are separated by an energy barrier. To pick up an atom the tip moves close to it and a negative bias is applied, as a result the potential well gets distorted in favor of the tip and when the tip moves away from the surface the atom will follow [28]. The drop off starts the same as pick up, the tip moves close to the surface, but now a positive bias is applied shifting the minimum potential well to the surface and leaving the atom on the surface.

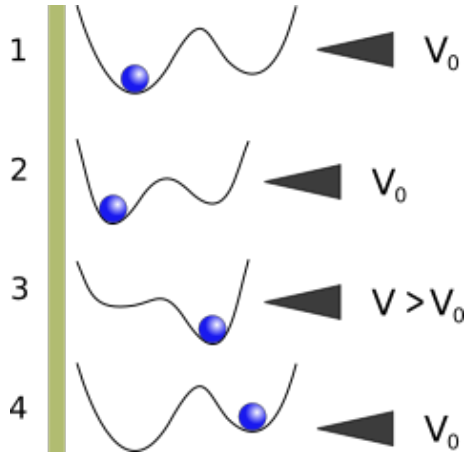


Figure 4.7: The schematic of picking up an atom explained by the double potential well. In (1) the tip is within imaging distance and the atom is still stable on the surface. As the tip gets closer the potential well gets distorted (2). Applying a bias voltage will favor the potential well of the tip and the atom will fall into it (3). When the tip is moved the atom will follow and the atom is picked up (4). Image adapted from reference [1]

4.2.2 Vertical atom manipulation on Cu_2N

Vertical atom manipulation has been applied on the more commonly used Cu_2N and spin structures have been built on this sample [1, 20]. This thesis determines the extent to which vertical atom manipulation on Cu_2N can be applied on Cu_3AuN_2 and the result of this are shown in section 5.2.1.

Vertical atom manipulation on Cu_2N consists of: Pick up, Drop off, and Hop. This is done as follows: After taking a topography the tip is positioned over an atom, shown in Figure 4.8a, with the feedback loop on. The tip's height will be at a fixed distance above the atom by setting it to a starting setpoint (50 pA, 20 mV). Next the feedback is turned off and the tip is lowered a few Ångström, after waiting for a few hundred milliseconds the voltage is increased to 1.1 V in order to transfer the atom to the tip. Finally the tip is retracted, the voltage is set back to the starting setpoint and the feedback is turned on, the result of a pick up can be seen in Figure 4.8b. Dropping off the atom is done in the exact same way as picking up, but now a negative transfer V_b is set.

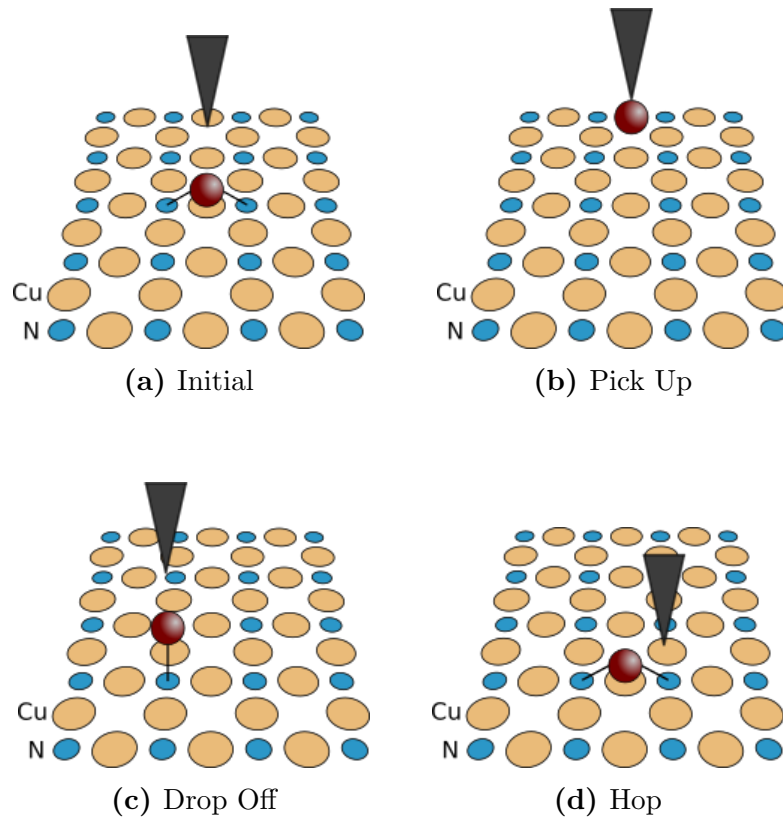


Figure 4.8: A visualization of vertical atom manipulation on Cu_2N lattice. **(a)** The Fe atom is in the lowest energy configuration sitting on top of a Cu atom and having two covalent bonds with the neighbouring N. **(b)** A bias voltage is applied breaking the covalent bonds of the Fe atom and the tip picks it up. **(c)** After being dropped off from the tip the Fe atom lands on a N atom forming a single covalent bond and leaving a single unpaired electron. In **(d)** the atom has hopped from the N atom to the Cu atom and forming two covalent bonds bringing it back to the lowest energy configuration. Images adapted from reference [1]

When an Fe atom is transferred from the tip to the surface the atom will always land on a N atom forming a single covalent bond, this configuration will leave the Fe atom with an unpaired electron, see Figure 4.8c. However this is not the lowest energy configuration, by placing the tip half a unit cell in the desired direction and applying a small voltage pulse the atom will hop onto a Cu atom forming two covalent bonds with the nitrogen, see Figure 4.8d

Chapter 5

Results

This chapter will cover the numerical simulation and experimental results. Section 5.3 will discuss a comparison of these results.

5.1 Numerical simulation results

This section will cover the results for a single atom and a trimer structures to verify the fidelity of the implementation of the Hamiltonian. Sections 5.1.3 and 5.1.4 will show illustrations of the individual atom population of the frustrated magnetic systems, the D7 and D9. Section 5.1.5 will cover the ESR simulations performed on a trimer.

The parameters used for the simulations correspond to Fe atoms on a Cu_2N crystalline lattice. By default these parameters are shown in Table 5.1 unless otherwise specified in the captions. The values are taken from [10, 22]

Table 5.1: The parameters used in the simulations. Spin s , g-factor g , uniaxial anisotropy D , transverse anisotropy E , N direction coupling J_1 , hollow direction coupling J_2 , diagonal coupling J_3 .

S	g	D (meV)	E (meV)	J_1 (meV)	J_2 (meV)	J_3 (meV)
2	2.11	-1.55	0.31	0.7	0.1	-0.7

5.1.1 Single atom (verification)

The single atom does not have any coupling terms and will be to verify the implementation of the anisotropy Hamiltonian. Expected from the anisotropy Hamiltonian is $D < 0$ causes a favoring of high $|m|$ spin states along z-axis and $E > 0$ mixes the states causing a zero field splitting of the states. The Zeeman term will cause the B-field in the N direction to favor the highest aligned state. A single Fe atom is a spin-2 system and has 5 m states (+2, +1, 0, -1, -2), Figure 5.1 shows the

evolution of the 5 corresponding eigenenergies (represented by the lines in the graph) with respect to B-field. The B-field is applied along the N direction (z), the hollow direction (x) and out-of-plane (y). It can be seen that the two lowest energies correspond to the highest $|m| = 2$ and the next highest correspond to $|m| = 1$ and at 0 T there is a splitting of the states. As the B-field increases in the N direction the $|+2\rangle$ is the most favorable and for high enough field $|+1\rangle$ will become more favorable than $|-2\rangle$. The B-field in the hollow and out-of-plane direction does not change the energies much.

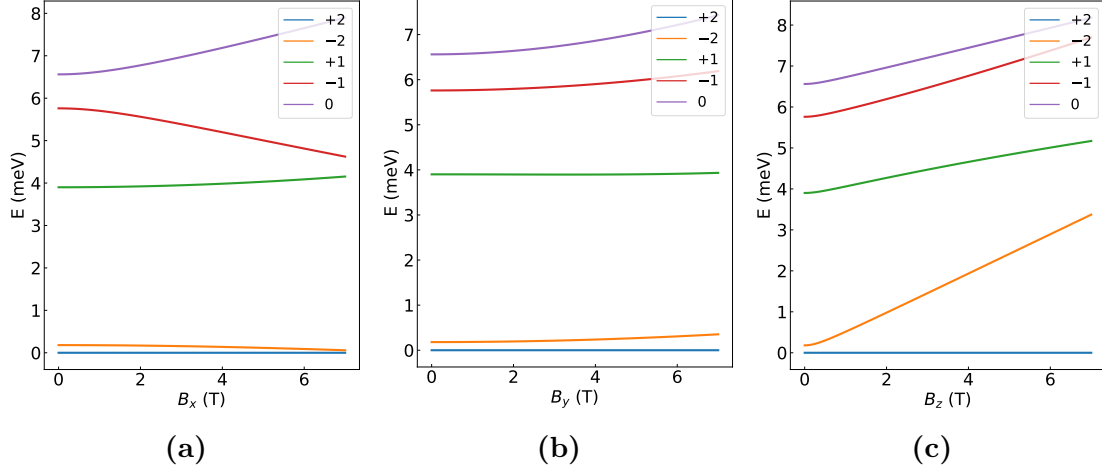


Figure 5.1: The evolution of the excitation energies with respect to field for a single Fe atom on Cu_2N . Here B_z is chosen along N direction **(c)**, B_x is chosen along the hollow direction **(a)** and B_y is chosen along the out-of-plane direction **(b)**.

In Table 5.2 are the eigenvectors for a single Fe atom at $B_z = 0$ T and $B_z = 7$ T in the basis $\hat{S}_z |m\rangle$. For $B = 0$ T the ground state $|\psi_0\rangle$ has the highest population in $|+2\rangle$ and $|-2\rangle$. It is possible to transition from the ground state to excited states with \hat{S}_x and \hat{S}_y . From the eigenvectors at 0 T $|\psi_0\rangle$ can transition to $|\psi_1\rangle$, $|\psi_2\rangle$, $|\psi_3\rangle$. The situation is different at 7 T, the ground state is now primarily in $|+2\rangle$ making transitions to $|\psi_2\rangle$, $|\psi_3\rangle$ visible and to $|\psi_1\rangle$, $|\psi_4\rangle$ not possible.

Table 5.2: The eigenvectors for a single Fe atom on Cu_2N , described by the anisotropy Hamiltonian Equation (2.6). They are shown for $B = 0$ T and $B = 7$ T along the N direction.

	$B_z = 0$ T					$B_z = 7$ T				
	$ +2\rangle$	$ +1\rangle$	$ 0\rangle$	$ -1\rangle$	$ -2\rangle$	$ +2\rangle$	$ +1\rangle$	$ 0\rangle$	$ -1\rangle$	$ -2\rangle$
$ \psi_0\rangle$	-0.697	0.000	0.166	0.000	-0.697	-0.995	0.000	0.097	0.000	-0.021
$ \psi_1\rangle$	-0.707	0.000	0.000	0.000	0.707	-0.036	0.000	-0.157	-0.000	0.987
$ \psi_2\rangle$	-0.000	0.707	0.000	-0.707	0.000	0.000	0.916	0.000	-0.402	-0.000
$ \psi_3\rangle$	0.000	0.707	0.000	0.707	0.000	-0.000	-0.402	-0.000	-0.916	0.000
$ \psi_4\rangle$	-0.117	0.000	-0.986	0.000	-0.117	-0.092	0.000	-0.983	0.000	-0.159

As the figures and table resulting from the simulation match the corresponding figures and table from reference [22] Figure 5.1c and Figure 5.1a match Figures 2c and 2d of [22] respectively. Table 5.2 matches Table 1. of [22] in terms of magnitude and relative phase, some minor discrepancies are due to a global phase and a ‘-’ sign in the Zeeman term. The fidelity of the simulation matches the reference.

5.1.2 Trimer (verification)

The Trimer composed of three coupled Fe atoms explores the interplay between anisotropy and coupling and verifies the implementation of the Heisenberg model in the simulation. Figure 5.2 shows the naming scheme of the trimer and the coupling between the atoms.

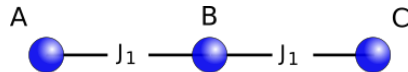


Figure 5.2: Visualization of the studied trimer. It is an open ended chain consisting of three atoms antiferromagnetically coupled with the N direction coupling J_1

The representation of the individual eigenstates will be done in color graphs and the idea was taken from reference [3]. Figure 5.3 shows the first two eigenvectors for a trimer at $B = 0$ T, where different anisotropy parameters have been turned off to see the role of the coupling between the atoms and the anisotropy of the spins. The trimer on a Cu_2N lattice is shown in Figure 5.3a at 0 T, it can be seen that the population is primarily in the high $|m\rangle$ and there is no preference between the $|+2\rangle$ and $|-2\rangle$. In Figure 5.3b the anisotropy parameter D , D_{ani} , is turned off, now the spin populates all the states. In Figure 5.3c the anisotropy parameter E , E_{ani} , is turned off, now it seems that the chain is aligning antiferromagnetically, however the energy of the first excited state is around the machine epsilon and therefore the

states are supposed to be degenerate. In Figure 5.3d both D_{ani} and E_{ani} are turned off, in this case as well the energy of the excited state is of the order of the machine epsilon making the two states degenerate and there is population in the lower $|m\rangle$ states.

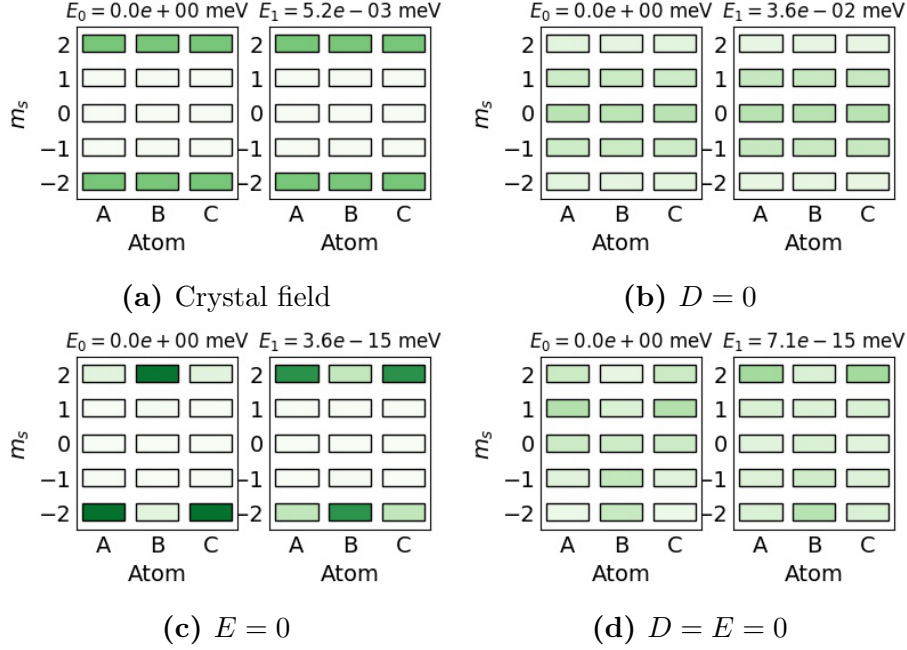


Figure 5.3: The population of the individual atoms for the first two eigenstates with corresponding eigenenergies of a Fe-trimer on a Cu_2N lattice at $B = 0 \text{ T}$ along N direction, the parameters used can be found in Table 5.1. The eigenstates are displayed for **(a)** the full crystal field, **(b)** when $D = 0$, **(c)** when $E = 0$ and **(d)** when $D, E = 0$. The representation idea was taken from reference [3].

Figure 5.4 shows the first two eigenstates of the trimer with the same variation in anisotropy, but now with a 500 mT field in the N direction. The trimer on a Cu_2N lattice, shown in Figure 5.4a, at 500 mT is now separated in the Neel states. At this field it is more favourable to satisfy the coupling than align all the atoms with the B-field. The groundstate is $|\uparrow\downarrow\uparrow\rangle$ and the first excited state is $|\downarrow\uparrow\downarrow\rangle$. The favoring of the spin to align with the magnetic field is stronger than the mixing of the E parameter. Figure 5.4b shows the same population as in the 0 T case, since the symmetry is not broken and the E parameter mixes the states, the magnetic field does not have an effect. Figure 5.4c is the same as with finite E parameter. With a finite magnetic field the antiferromagnetic coupling is more visible in Figure 5.4d, and all of the states are used for the antiferromagnetic coupling.

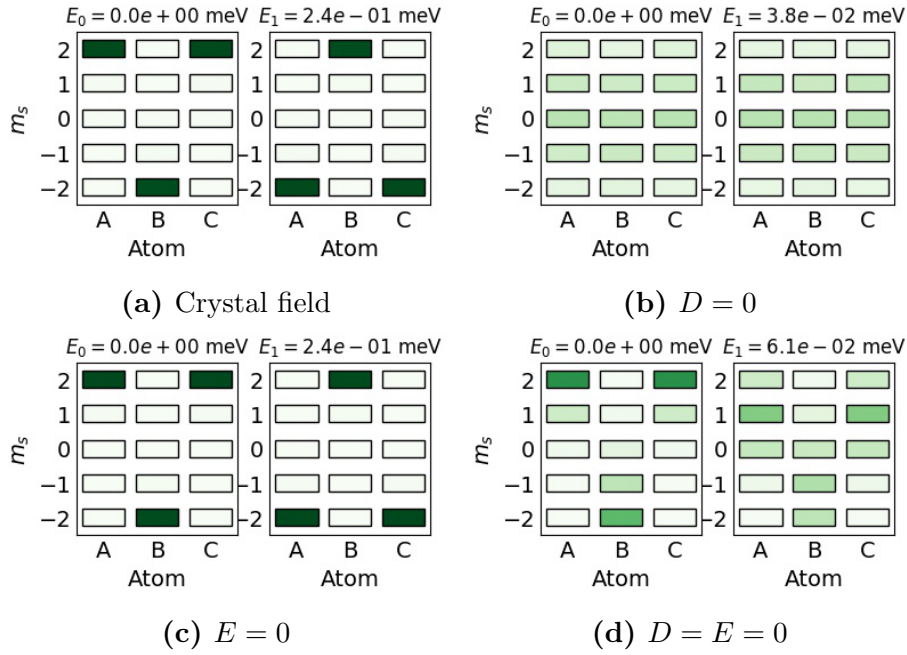


Figure 5.4: The population of the individual atoms for the first two eigenstates with corresponding eigenenergies of a Fe-trimer on a Cu_2N lattice at $B = 500$ mT along N direction, the parameters used can be found in Table 5.1. The eigenstates are displayed for (a) the full crystal field, (b) when $D = 0$, (c) when $E = 0$ and (d) when $D, E = 0$.

No references were found for the trimer, hence we can't check the simulation results against previous research. The simulation results regarding the behaviour of the couplings meet expectations. Hence this will be used for the simulation of the frustrated systems.

5.1.3 A frustrated 7 atom structure: D7

Figure 5.5 shows the naming scheme of the D7 structure and the coupling between the atoms. The vertical (J_1) and horizontal (J_2) couplings are antiferromagnetic, while the diagonal coupling J_3 is ferromagnetic. The following relations hold $|J_1| > |J_2|$ and $|J_1| = |J_3|$.

The first four eigenstates of the D7 are displayed in Figure 5.6 at $B = 0$ T along the N direction. From D_{ani} the population of the atoms are primarily in $|+2\rangle$ and $|-2\rangle$ states and E_{ani} causes a mixing of the states and not being able to recognize a difference in population.

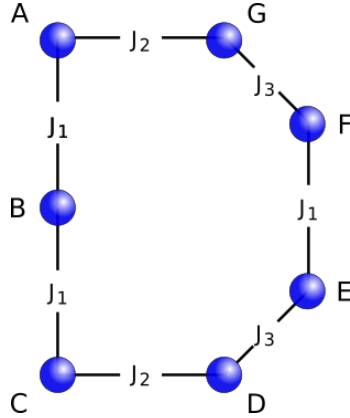


Figure 5.5: Visualization of the magnetically frustrated D7. It is a closed chain consisting of 7 atoms both antiferromagnetically (J_1 and J_2) and ferromagnetically (J_3) coupled according to the orientation of the atoms. The values for the couplings can be found in Table 5.1.

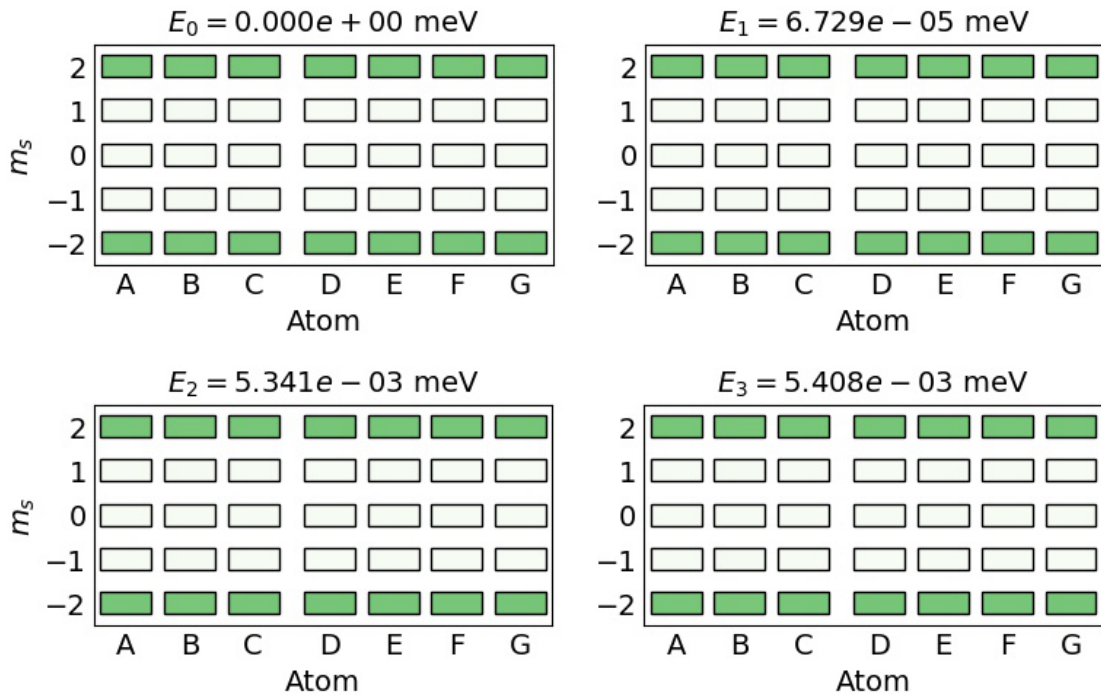


Figure 5.6: The population of the individual atoms for the first four eigenstates with corresponding eigenenergies of a Fe-D7 on a Cu₂ lattice at $B = 0$ T. The white space separating atom ‘C’ and ‘D’ is to indicate the weak coupling, which is also present between atom ‘G’ and ‘A’.

When a magnetic field is applied the D7 starts to split up in two section ‘A-B-C’ and ‘D-E-F-G’, the first four eigenstates are displayed in Figure 5.7. The separation

into two sections is caused by the weak coupling between atoms ‘C’ and ‘D’ and atoms ‘G’ and ‘A’, the weakest coupling determines the frustration release point since it costs the least amount of energy. Therefore the D7 splits up in three atom chain and a four atom chain. Like the trimer at this field ‘A-B-C’ is fixed for the ground state $|\uparrow\downarrow\uparrow\rangle$ and satisfying the coupling requirement is more favourable than aligning all three with the magnetic field. The other part (D-E-F-G) is unaffected by the field, because $|\uparrow\uparrow\downarrow\downarrow\rangle$ is as energetically favorable as $|\downarrow\downarrow\uparrow\uparrow\rangle$. The frustration release point can still be between ‘C-D’ or ‘G-A’. The second and third excited state have the trimer flipped, where two spins are against the magnetic field and the same configuration for ‘D-E-F-G’.

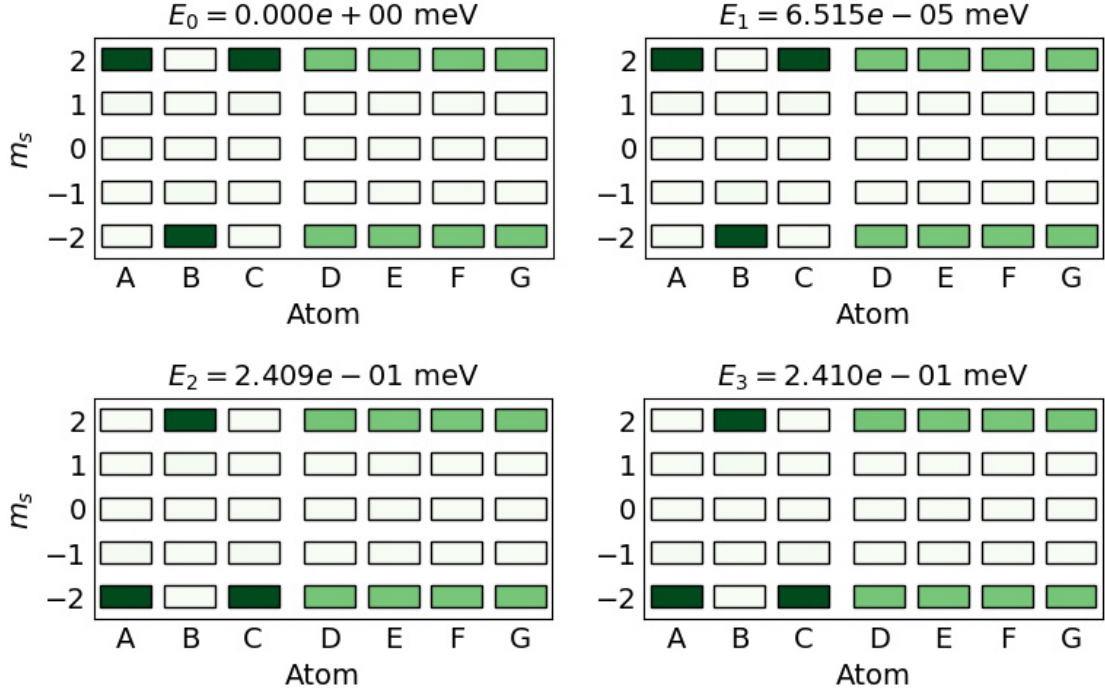


Figure 5.7: The population of the individual atoms for the first four eigenstates with corresponding eigenenergies of a Fe-D7 on a Cu_2 lattice at $B = 500$ mT. The white space separating atom ‘C’ and ‘D’ is to indicate the weak coupling, which is also present between atom ‘G’ and ‘A’.

For the experiment, the D7 will have the symmetry breaking of D-E-F-G, according to [10] D_{ani} can vary up to 20% depending on the precise positioning of the neighboring atom. To induce this symmetry break, D_{ani} on atom ‘D’ will be reduced by 2%. The result is shown in Figure 5.8, where the first four eigenstates are displayed. For the ground state the magnetic frustration is located between atom ‘C’ and ‘D’, while the first excited state has the frustration between ‘G’ and ‘A’. Since $|D_{ani}|$ is lowered on atom ‘D’, the requirement for the population to be in the high $|m\rangle$ is less strict than for the other atoms. This means that more population can be higher

in the $|+1\rangle$ and $|−1\rangle$ for atom ‘D’ to decrease the frustration of not fulfilling the coupling requirement. In the second and third excited state the trimer is flipped and also in this case the frustration is between atoms ‘C’ and ‘D’ is more favorable than between ‘G’ and ‘A’.

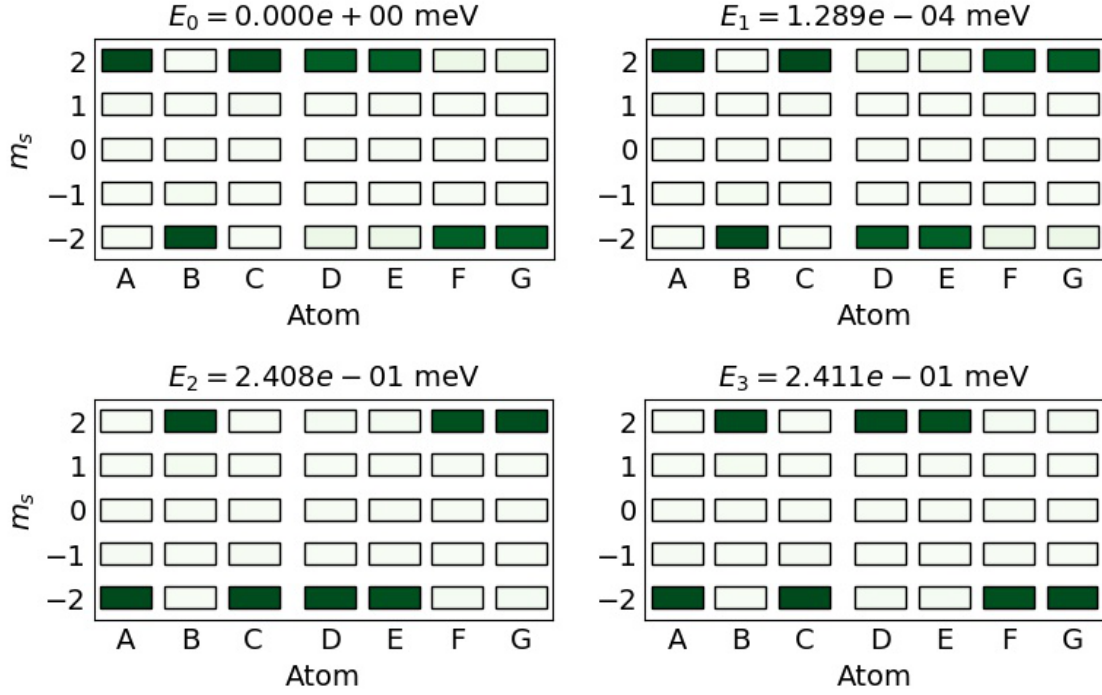


Figure 5.8: The population of the individual atoms for the first four eigenstates with corresponding eigenenergies of a Fe-D7 on a Cu_2 lattice at $B = 0 \text{ T}$. On atom ‘D’ an anisotropy parameter of $D = -1.519 \text{ meV}$ was used. The white space separating atom ‘C’ and ‘D’ is to indicate the weak coupling, which is also present between atom ‘G’ and ‘A’.

Atom ‘D’ has a reduced D_{ani} , so the population in the $|\pm 1\rangle$ is higher than for the other atoms. As a result the coupling penalty will be lower for ‘C-D’ than for ‘G-A’, but when increasing the B-field at a certain point it will be more favourable to have the highest amount of spin aligned with the field. In this case ‘F-G’ will align along the field and ‘D-E’ against the field, thereby making the first excited state from Figure 5.8 more favourable than the ground state. This switching of ground state and excited state also holds for increased D_{ani} on atom ‘D’, and is explained in the next paragraph. The tipping point for different D_{ani} and E_{ani} on atom ‘D’ are shown in Figure 5.9. In this Figure a maximum B-field of 5 T was chosen, so points in the graph at 5 T have not switched states. It can be seen that having a large difference in ratio of D_{ani} or E_{ani} causes the switch to happen at low B-fields, so switching the ground state controllably would be possible by applying a B-field.

Taking a few examples, where D_D is D_{ani} of atom ‘D’: at $D_D/D_{ani} = 1$ and $E_D/E_{ani} = 1$ the whole chain is symmetric and the situation would be the same as in Figure 5.6 and no switching will occur.

At $D_D/D_{ani} = 1.04$ and $E_D/E_{ani} = 1$ for low field atom D wants to be more in the $|\pm 2\rangle$ state so the frustration release will be in ‘G-A’, because the coupling penalty is lower. For higher field it is more favourable to have the highest amount of spin aligned with the field, since atom ‘D’ has more population in $|\pm 2\rangle$, it will align with the field and the frustration will occur in ‘C-D’. Thereby switching the favourable state.

At $D_D/D_{ani} = 1$ and $E_D/E_{ani} = 1.04$ for low field atom D has more mixing between the $|m\rangle$ states, therefore it has lower population in $|\pm 2\rangle$ and the frustration release will be in ‘C-D’, because the coupling penalty is lower. For higher field it is more favourable to have the highest amount of spin aligned with the field. Since atom ‘D’ has lower population in $|\pm 2\rangle$, atoms ‘F’ and ‘G’ will align with the field and the frustration will occur in ‘G-A’. Thereby switching the favourable state.

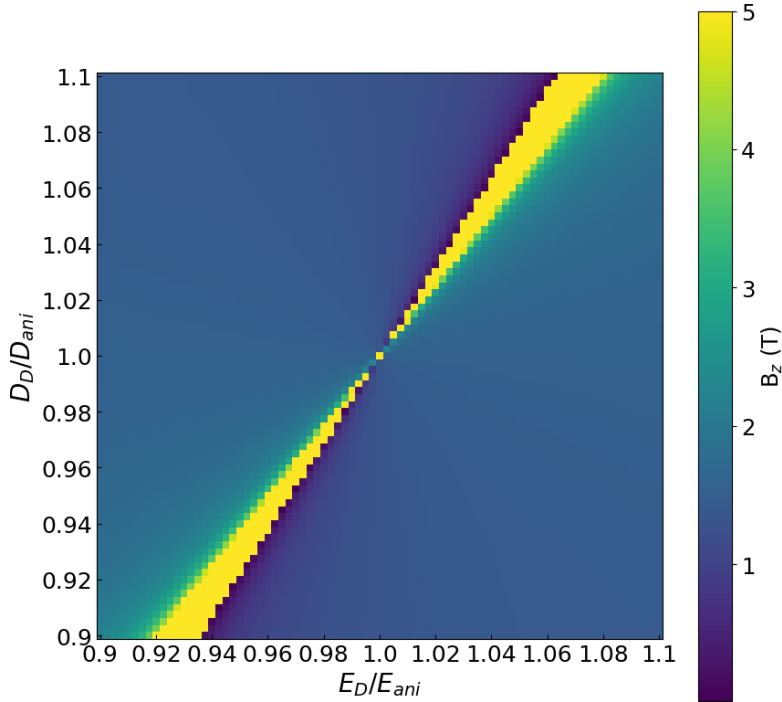


Figure 5.9: The B-field required to counterbalance the effect of the varying anisotropy on atom ‘D’.

5.1.4 A frustrated 9 atom structure: D9

The naming scheme for the following simulation results are displayed in Figure 5.10. The couplings for the D9 are: The vertical (J_1) and horizontal (J_2) couplings are antiferromagnetic, while the diagonal coupling J_3 is ferromagnetic. The same relations

as the D7 hold, $|J_1| > |J_2|$ and $|J_1| = |J_3|$.

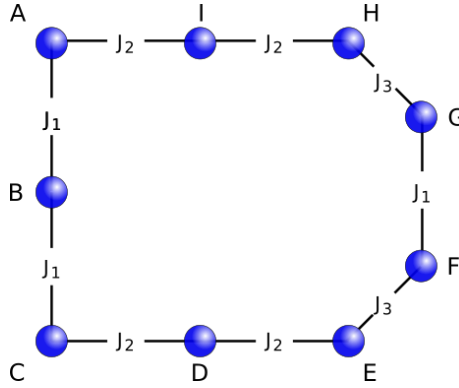


Figure 5.10: Visualization of the magnetically frustrated D9, it is a closed chain consisting of 9 atoms both antiferromagnetically (J_1 and J_2) and ferromagnetically (J_3) coupled according to the orientation of the atoms. The values for the couplings can be found in Table 5.1.

The first four eigenstates of the D9 are displayed in Figure 5.11 at $B = 0$ T. This behaves the same as the the D7 the population of the atoms are primarily in $|+2\rangle$ and $|-2\rangle$ states because of D_{ani} and E_{ani} causes a mixing of the states and not being able to recognize a difference in population.

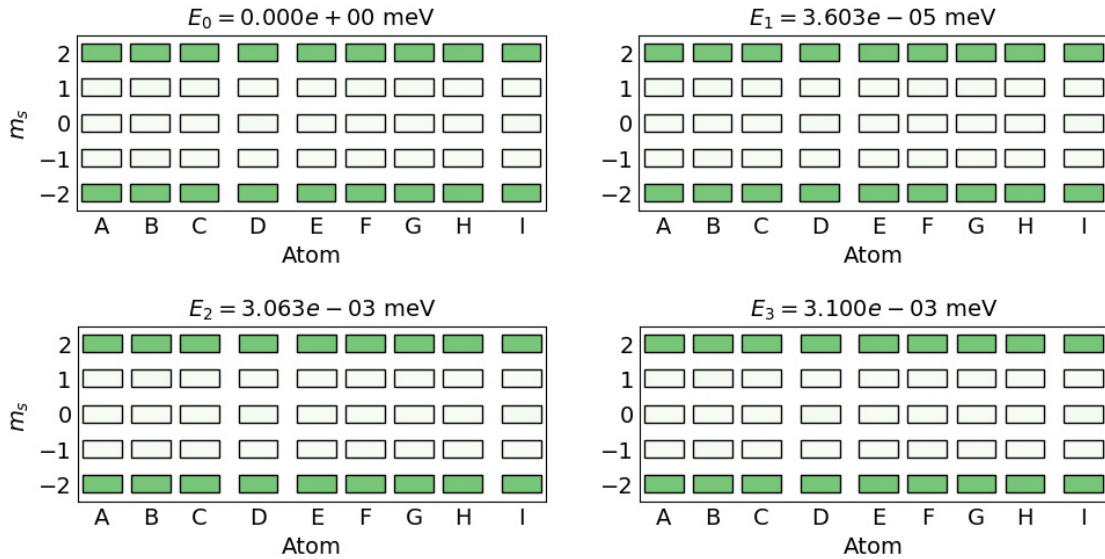


Figure 5.11: The population of the individual atoms for the first four eigenstates with corresponding eigenenergies of a Fe-D9 on a Cu_2 lattice at $B = 0$ mT. The white space separating atoms 'C-D-E' and atoms 'H-I-A' is to indicate the weak coupling.

Now with the D9 there are 4 frustration release points: 'C-D', 'D-E', 'H-I' and 'I-A'.

When a magnetic field is applied the first two states of the D9 splits up in two sections ‘A-B-C’ and ‘D-E-F-G-H-I’, where ‘A-B-C’ is fixed like the trimer and the other part is like the D7 unaffected by the field and in superposition between $|\pm 2\rangle$ shown in Figure 5.12. In this case it would not be energetically favourable for atom D and I to be against B-field to satisfy the coupling of the neighbouring atoms. The situation is different for the second and third excited states, now ‘A-B-C’ is flipped and atoms ‘D’ and ‘I’ can satisfy the coupling and alignment with the magnetic field.

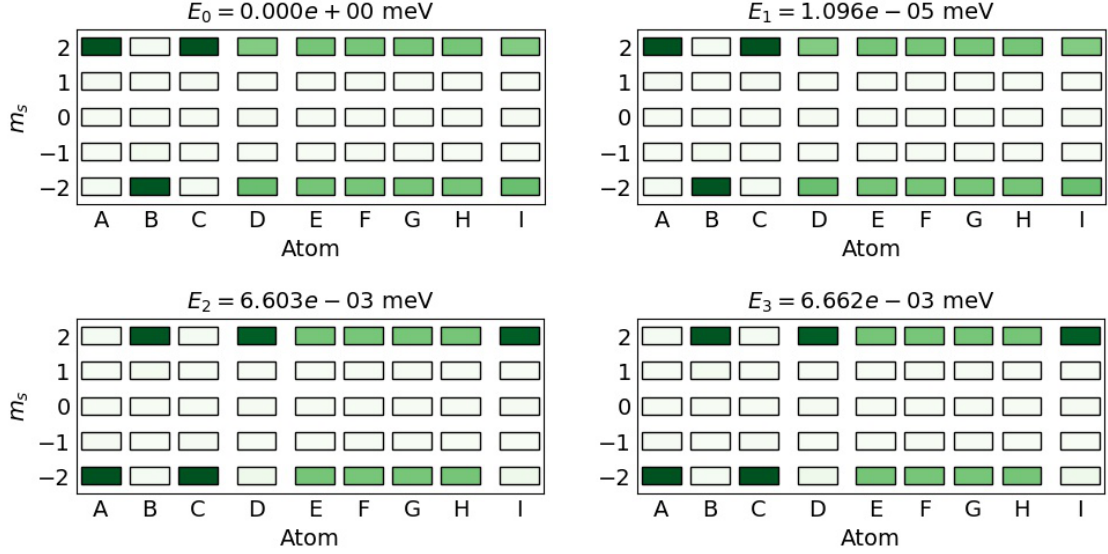


Figure 5.12: The population of the individual atoms for the first four eigenstates with corresponding eigenenergies of a Fe-D9 on a Cu_2 lattice at $B = 500$ mT. The white space separating atoms ‘C-D-E’ and atoms ‘H-I-A’ is to indicate the weak coupling.

For the experiment, the D9 will have symmetry breaking of ‘D-E-F-G-H-I’, just like the D7 the symmetry will be broken by reducing D_{ani} by 2% on atom ‘D’. As a result the frustration release will be in ‘C-D’, because the population of atom ‘D’ in $|\pm 1\rangle$ can be higher than the other atoms and therefore decreases the frustration of not fulfilling the coupling requirement. In the second excited state the frustration has moved to ‘D-E’ still only paying J_2 as penalty. In the third excited state the frustration has moved to ‘H-I’.

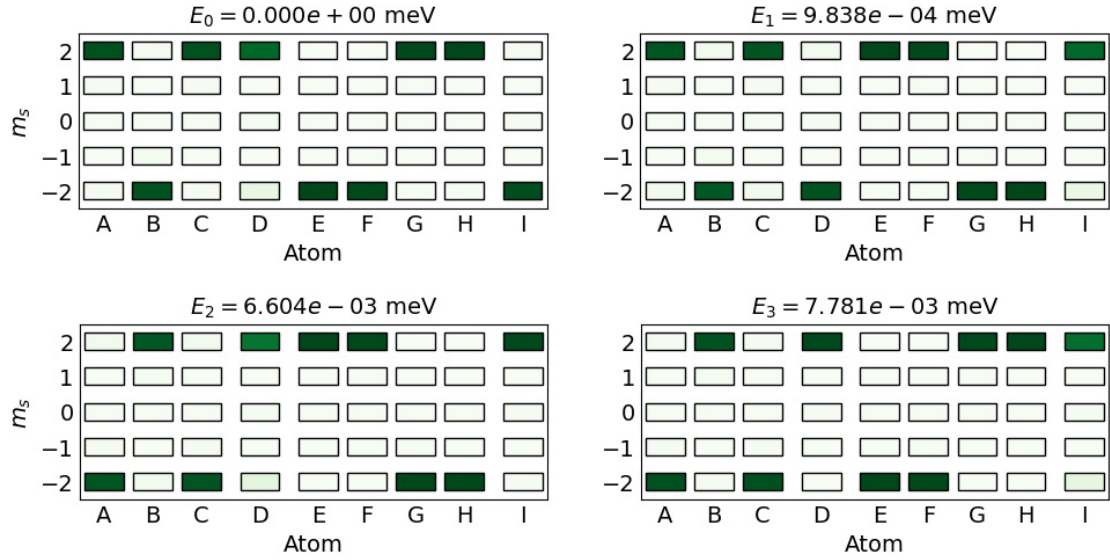


Figure 5.13: The population of the individual atoms for the first four eigenstates with corresponding eigenenergies of a Fe-D9 on a Cu₂ lattice at $B = 500$ mT. On atom ‘D’ an anisotropy parameter of $D = -1.519$ meV was used. The white space separating atoms ‘C-D-E’ and atoms ‘H-I-A’ is to indicate the weak coupling.

5.1.5 ESR

As stated before in section 4.1.6, an ESR measurement has a high energy resolution. It is shown from the simulations in Figure 5.8, that the first excitation energy of the frustrated D7 is very small; Therefore it would benefit from ESR measurements to determine state transitions instead of using STM-IETS.

The numerical simulator can be used to predict the excitation energy required to excite the studied spin-coupled systems and is currently (while writing this thesis) being used in the labs to predict the necessary excitation frequency. The Ottelab group will be the first to test ESR on Cu₃AuN₂ surface and will be done on a simple structure to demonstrate the feasibility.

This thesis will show a prediction of the excitation energy for a trimer seen in Figure 5.2. In an ESR experiment the tip can influence the excitation energy, because the local field of the tip is able to cancel the external field when probing an atom. The influence of this on the excitation frequency is shown in Figure 5.14. The Figure only shows the top and middle atom being probed, since probing the top or the bottom atom is symmetric.

It can be seen that probing the top atom is symmetric around $B_z = 0$ T, the cause for this is that the probed atom will align with the local field and the other

two atoms are unaffected by the global field (the energies of $|\uparrow\downarrow\rangle$ and $|\downarrow\uparrow\rangle$ are the same).

Probing the middle atom causes an increase in excitation energy as the local field is reduced. The ground state will be $|\uparrow\downarrow\uparrow\rangle$ and the first excited state will be $|\downarrow\uparrow\downarrow\rangle$, so if the local field on the middle atom decreases then the Zeeman effect will favour the ground state more, since the middle atom of the ground state will align with the local field.

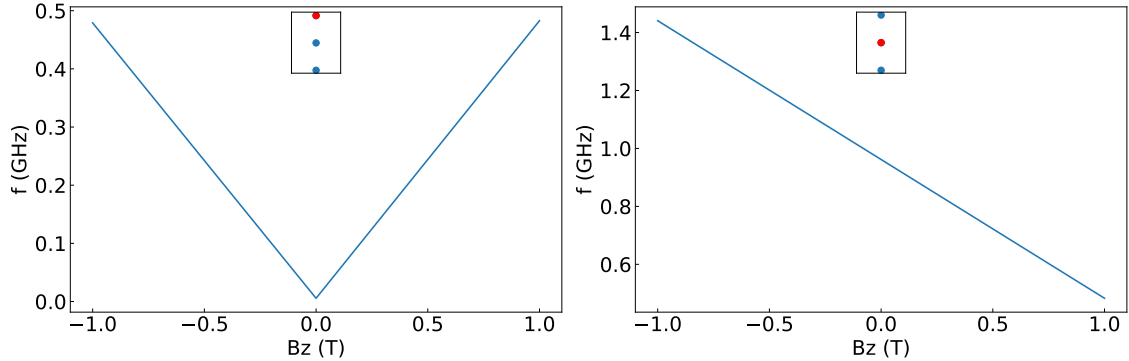


Figure 5.14: The frequency needed to excite the trimer from the ground state to the first excited state at a global B_z -field of 1 T on the blue atoms and a tip induced field sweep on the red atom.

5.2 Experimental results

This section will cover the results of the frustrated magnetic systems. Section 5.2.1 covers the progress in atom manipulation and built structures. The topography, spectroscopy and telegraphic noise is shown in section 5.2.2. All of the images were taken at $T = 330$ mK

5.2.1 Atom manipulation process and built structures.

In order to study a frustrated magnetic system, it has to be built first and a lot of time was spent in getting reliable vertical atom manipulations. The problem is that fine tuning the parameters for pick up, drop off and hop are tip shape and/or composition dependent, this means a failed atom manipulation can happen at any of the three stages.

A failed pick up can be dropping atoms from the tip onto the atom, thereby making it unusable as building block. The atom can migrate up the tip during a pick up, caused by a too aggressive bias voltage or the shape of the tip does not allow the atom to be on the apex. For a failed drop off either nothing drops or a cluster of

atoms drops from the tip, the last one changes the tip and also changes the manipulation parameters. A failed hop can be picking the atom up, dropping something on top of it or not hopping in the desired direction. Of which the last one occurred the most.

A few methods were found that increased the success rate for this sample and tip combination. To increase pick up rates the tip preparation was done until the imaged Fe atoms looked round, this ensures that the interference from other apexes is minimal. Additionally the bias voltage needs to be fine tuned so the Fe sits on the apex. For drop off it is important that the pick up was successful in other words the Fe atom is on the apex, because either nothing will drop or a different atom/-cluster could drop from the tip causing a tip change. For the hop the biggest issue was hopping the atom in the desired direction, the hopping direction determines the coupling strength, so atoms had to be hopped in specific directions. The biggest factor that influenced the direction was the hopping location on the insulating layer of the sample. An atom that only hopped horizontally on a N-island could be hopped vertically just by moving to a different part of the same island, sometimes as little as a few nm.

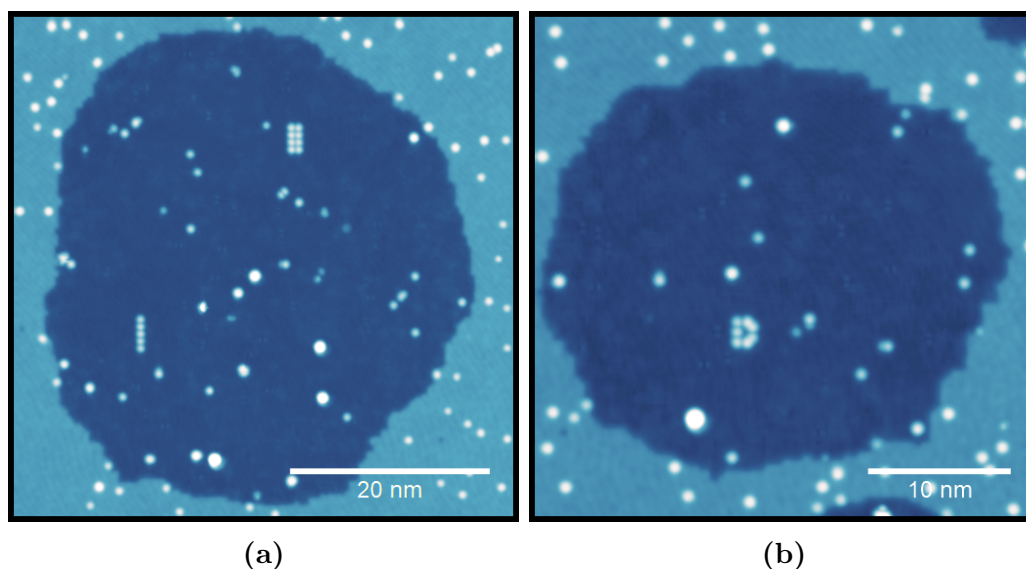


Figure 5.15: Images of spin structures made from Fe atoms, assembled through vertical atom manipulation and located on a $\sim 40 \times 30 \text{ nm}^2$ and $\sim 30 \times 30 \text{ nm}^2$ nitrogen island. **(a)** The 5 chain and 4×2 structures as in [4]. **(b)** The frustrated D7. Both images taken at 50 mV and 50 pA.

At the start it would typically take a week to get a successful atom manipulation and up to a month to create a single structure. By applying the aforementioned techniques the success rate increased to building multiple structures in a single day. The successful engineered spin structures on the nitrogen island are shown in

Figure 5.15 and a zoom-in of the spin structures in Figure 5.16. This shows that vertical atom manipulation on Cu_3AuN_2 works the same as on Cu_2N .

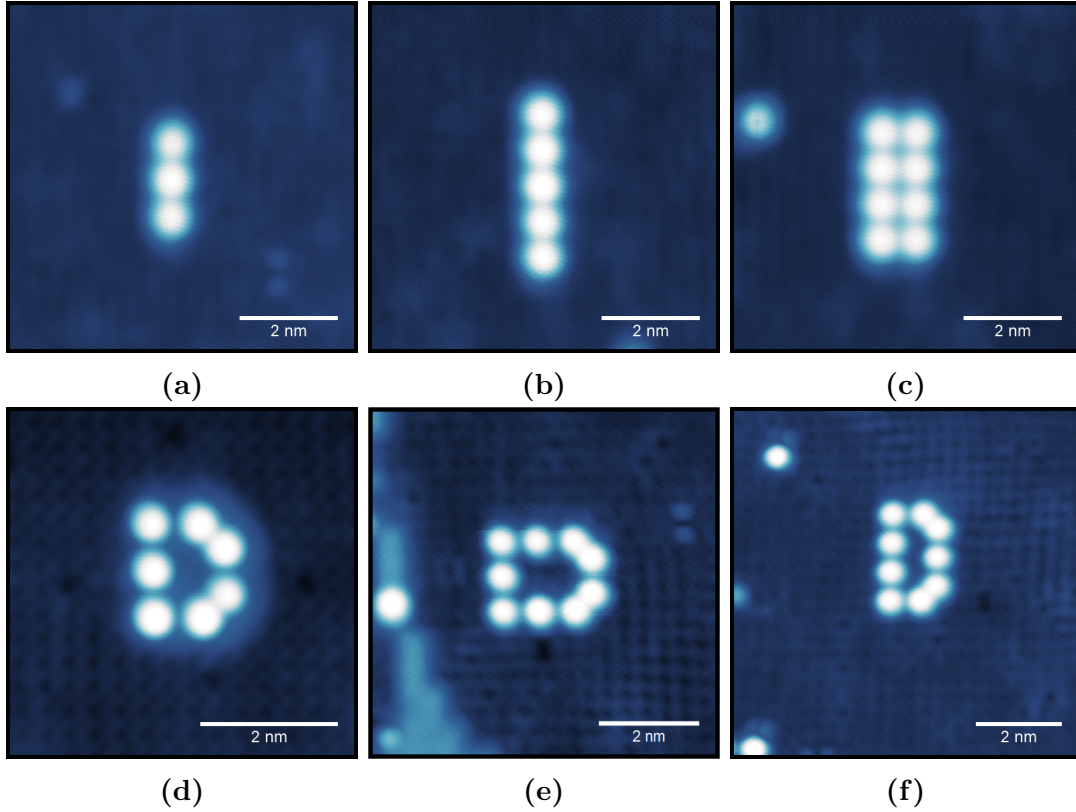


Figure 5.16: Images of the built spin structures made from Fe atoms and assembled through vertical atom manipulation. (a) 3 atom chain (trimer), (b) 5 atom chain, (c) 4 x 2, (d) Frustrated D7, (e) horizontal frustrated D9 and (f) vertical frustrated D9. Images taken at 50 pA and (a), (b), (c) 50 mV and (d),(e),(f) 20 mV

5.2.2 Measurements of a frustrated D7 structure

The topographic images of the D7 are scanned with a spin-polarized tip at different setpoints, shown in Figure 5.17. The polarization of the spin structure is visible in Figure 5.17a, which shows that the ground state is $|ABCDEF G\rangle = |\uparrow\downarrow\uparrow\uparrow\downarrow\downarrow\rangle$ and the frustration occurs between atoms ‘C’ and ‘D’. The weak couplings in the D7 are the points of frustration release and the structure will be considered as two weakly coupled parts, namely ‘A-B-C’ and ‘D-E-F-G’. The magnetic field favours $|\uparrow\rangle$ over $|\downarrow\rangle$, so ‘A-B-C’ is affected and as a result $|\uparrow\downarrow\uparrow\rangle$ has a lower energy than $|\downarrow\uparrow\downarrow\rangle$. ‘D-E-F-G’ on the other hand is unaffected by the magnetic field since both states have the same amount of atoms aligned with the B-field, so the energies of $|\uparrow\uparrow\downarrow\downarrow\rangle$ and $|\downarrow\downarrow\uparrow\uparrow\rangle$ are identical. The symmetry of the states is broken, because as stated before D_{ani} can vary up to 20% depending on the precise positioning of the neighbouring atoms. This also means that a D7 could be built with the ground

state having the frustration in ‘G-A’, however it has only been observed in ‘C-D’ from the three D7’s that were built.

At higher setpoints in Figures 5.17b - 5.17d a shadow starts to form starting at atom ‘E’ and growing towards atom ‘D’. The shadow is the result of the atoms alternating rapidly between two opposite magnetic states. The switching occurs due to the interaction between the tip and the atoms during a scan of the surface and this forces the $|\downarrow\rangle$ to be more favourable. In the case of the D7 the tip is not able to excite ‘A-B-C’, but provides enough energy to switch ‘D-E-F-G’.

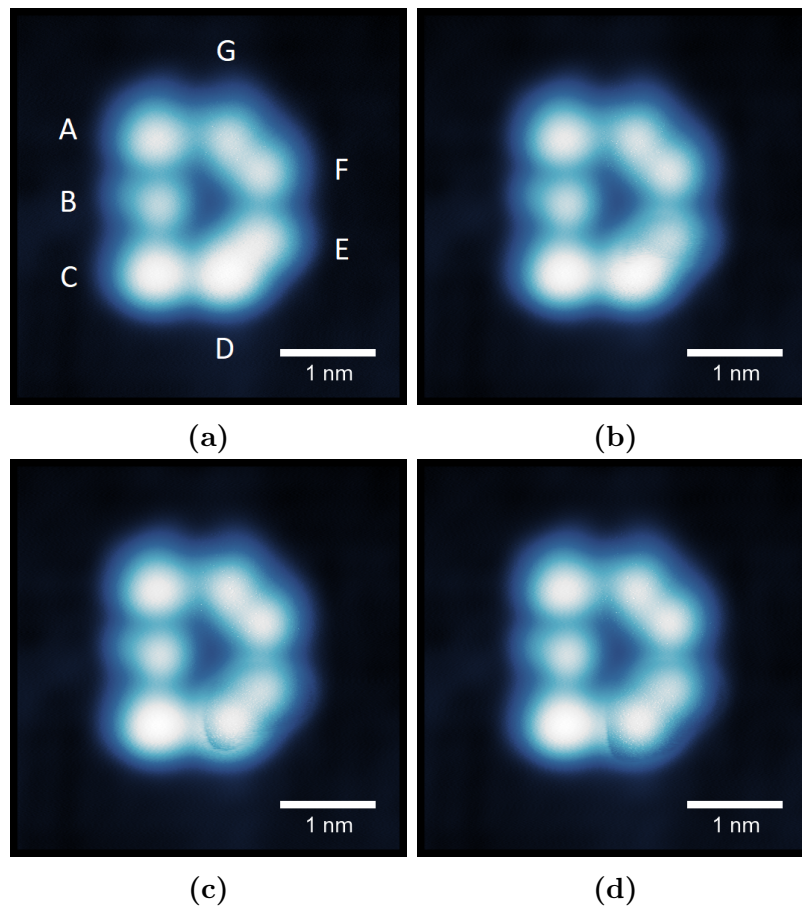


Figure 5.17: Images taken with a spin-polarized tip of the D7 structure at 1 T, 2 mV and (a) 50 pA, (b) 100 pA, (c) 150 pA, (d) 200 pA. The naming scheme of the atoms is visible in (a). Notice the shadow occurring at higher setpoints in atoms ‘D’ and ‘E’

The spin-polarized IETS measurement for a D7 was obtained by measuring each individual atom at a fixed tip height and the result is combined in Figure 5.18. Transitions to excited states are represented by a peak and immediately followed by a valley or the other way around instead of increasing and levelling as in Figure 4.4a,

this is the result of interaction with the spin-polarized tip [29]. For the peak-valley the spin of the atom starts of parallel with the tip (high conductance) and then at the excitation energy the atom is flipped causing it be anti-parallel (low conductance). The peaks and valleys become more pronounced as the setpoint increases from Figure 5.18a to Figure 5.18b, which is also consistent with reference [29].

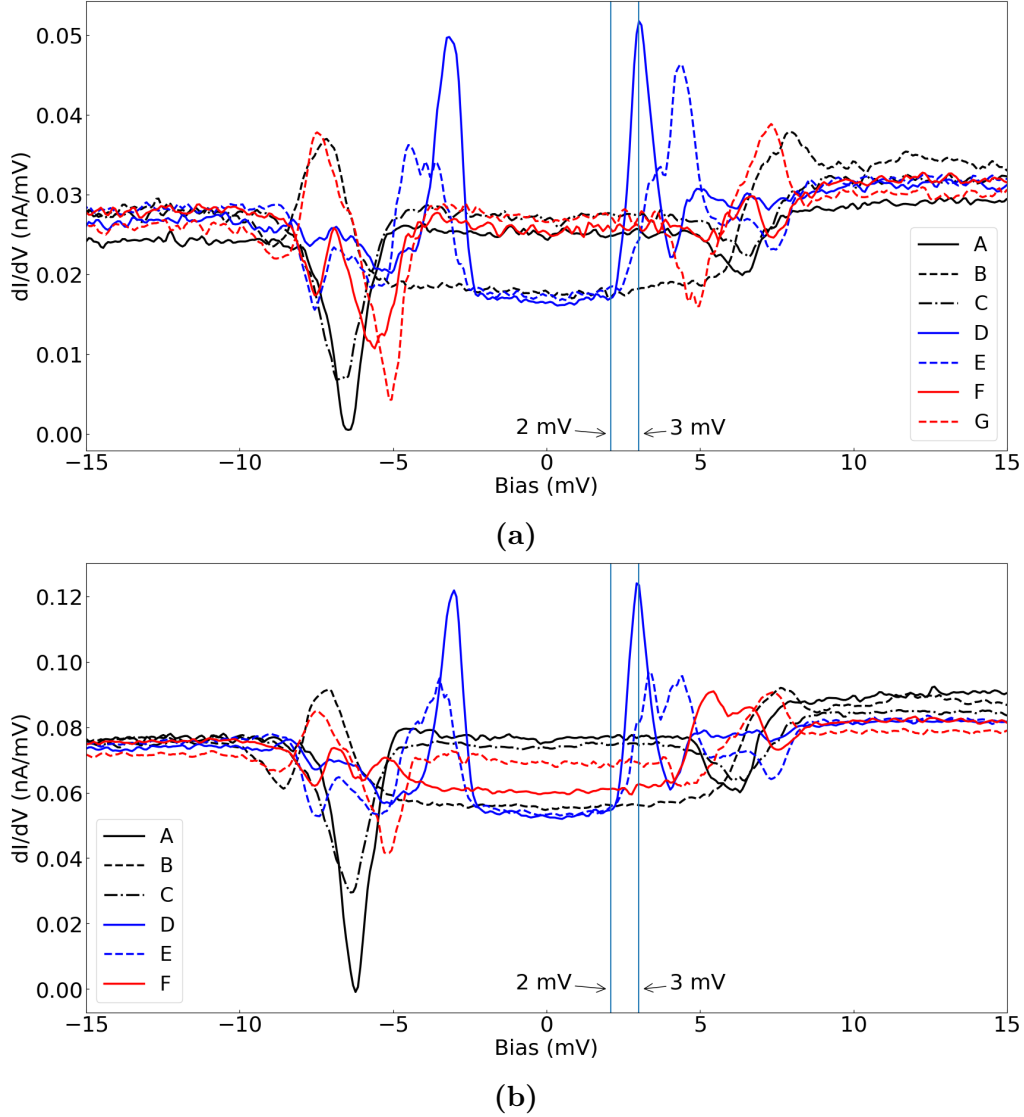


Figure 5.18: Spin-polarized spectroscopy of the individual atoms from a D7 at 1 T and a setpoint of 20 mV and (a) 500 pA, (b) 1 nA. The naming scheme in the legend follows the one in Figure 5.17a and the color scheme follows the different sections of the D7. There are two lines at 2 mV and 3 mV indicating the first excitation for atom ‘D’ and ‘E’.

The first transition of the D7 starts in Figure 5.18a between 2 mV and 3 mV, where both atoms ‘D’ and ‘E’ are starting to be excited. This is consistent with Fig-

ure 5.17, where the atoms ‘D’ and ‘E’ start switching between two different states. At higher bias the other atoms start to transition to excited states, ‘F’, ‘G’ at 5 mV, and ‘A’, ‘B’, ‘C’ at 7 mV.

The final measurement is done by measuring the current over time with a spin-polarized tip, the feedback is turned off and the setpoint is fixed, shown in Figure 5.19. These are converted to histograms of current versus time for readability. If the atom stays in one state then the current distribution will be a Gaussian around the current setpoint as can be seen for atoms ‘A’, ‘B’ and ‘C’ in Figure 5.20. If the atom switches between two states then the current distribution will be two Gaussians centered around the current values of tip-atom interaction being parallel or anti-parallel aligned.

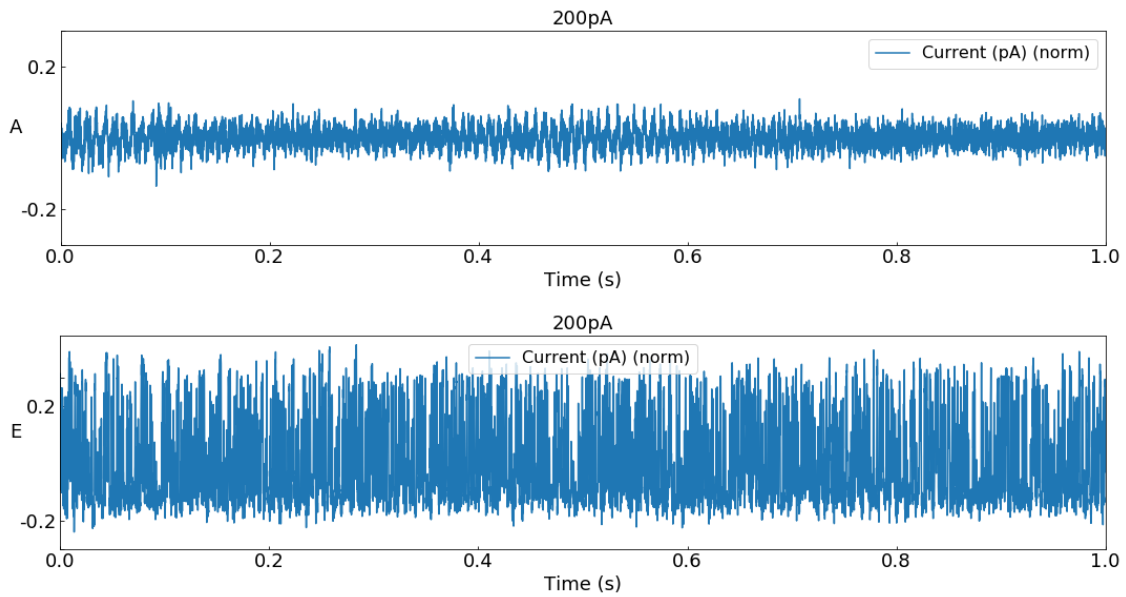


Figure 5.19: Normalized current time traces taken with a spin-polarized tip at 3 mV and 1 T for atoms ‘A’ and ‘E’. The title contains the current setpoint and each row is labeled by the corresponding atom. The current is centered around the setpoint and for atom ‘A’ at 200 pA, the y-axis should be read as $y \in [199.8, 200.2]$ pA

Atom ‘E’ in Figure 5.21 is in a single state at 50 pA and as the current increases a second peak appears, showing that it switches between two states. This behaviour is not as clear in atom ‘D’, but a second peak does appear. It seems to be switching much faster than atom ‘E’ not living in one state for long. The switching in these atoms are consistent with Figure 5.17 and Figure 5.18

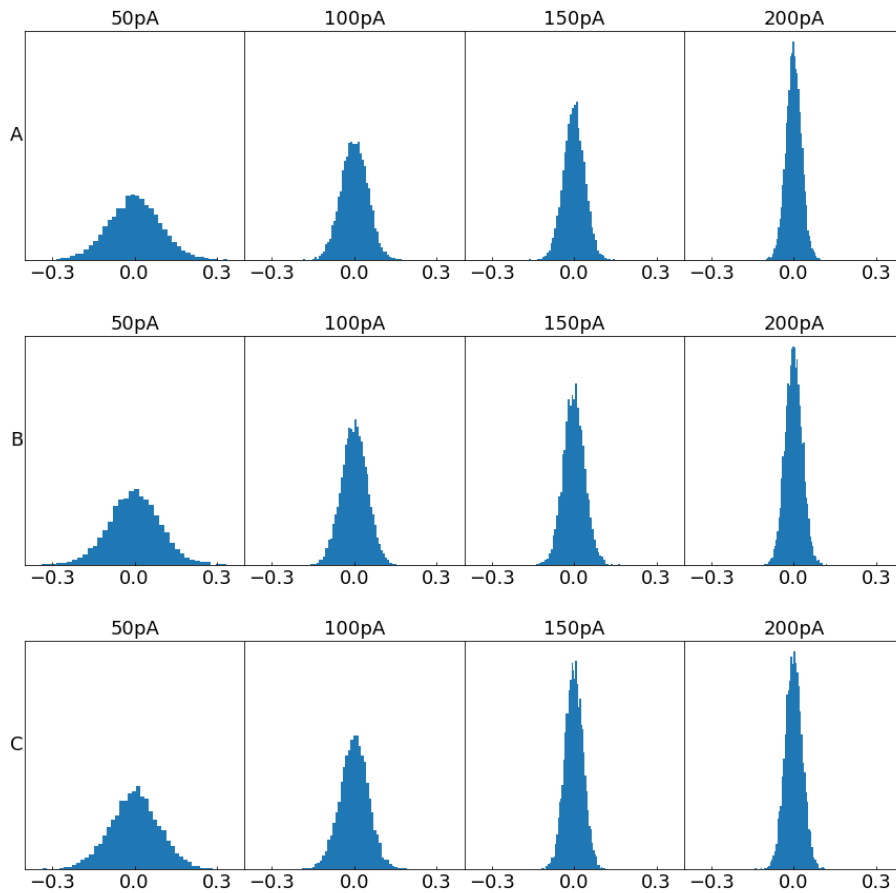


Figure 5.20: Normalized histograms of the current versus time taken with a spin-polarized tip at 3 mV and 1 T for atoms ‘A’, ‘B’ and ‘C’. The title contains the current setpoint and each row is labeled by the corresponding atom. The histogram is centered and for atom ‘A’ at 50 pA, the x-axis should be read as $x \in [49.7, 50.3]$ pA

Atoms ‘F’ and ‘G’ in Figure 5.22 at 200 pA start to show an indication of switching. As the tip is not perfectly polarized, it is still able to excite ‘F’ and ‘G’. However this is short lived, because the $|\downarrow\rangle$ is more favourable.

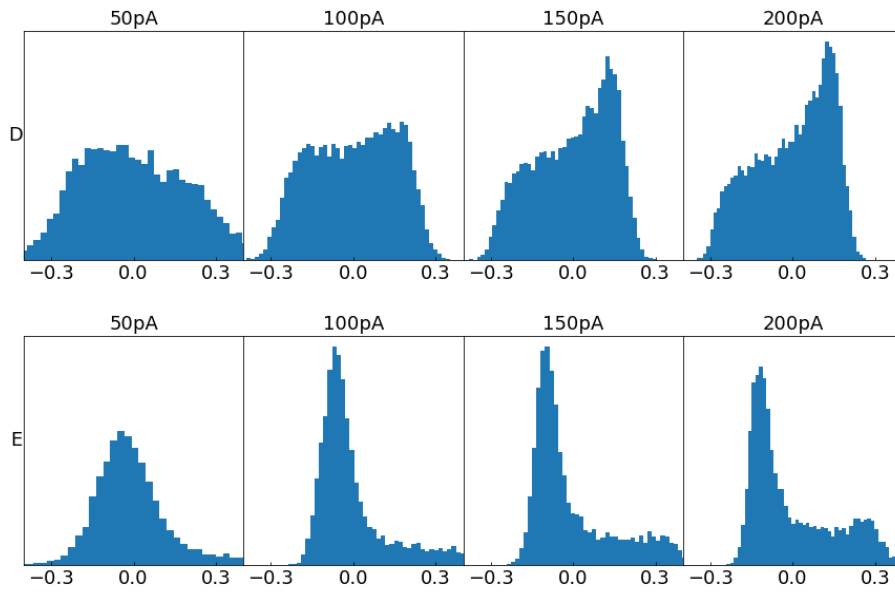


Figure 5.21: Normalized and centered histograms of the current versus time taken with a spin-polarized tip at 3 mV and 1 T for atoms ‘D’ and ‘E’. The title contains the current setpoint and each row is labeled by the corresponding atom.

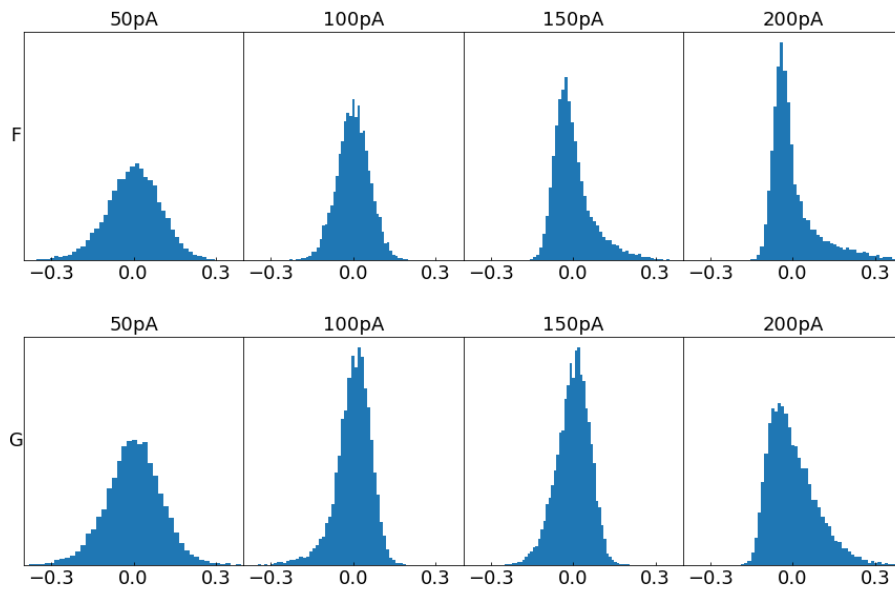


Figure 5.22: Normalized and centered histograms of the current versus time taken with a spin-polarized tip at 3 mV and 1 T for atoms ‘F’ and ‘G’. The title contains the current setpoint and each row is labeled by the corresponding atom.

5.3 Comparison of Simulation and Experimental Results

From Figure 5.8 the expectation is that: The first transition from the ground state will be $|ABC\ DEFG\rangle = |\uparrow\downarrow\uparrow\ \uparrow\uparrow\downarrow\downarrow\rangle \Rightarrow |ABC\ DEFG\rangle = |\uparrow\downarrow\uparrow\ \downarrow\downarrow\uparrow\uparrow\rangle$, where ‘D-E-F-G’ have flipped, due to the very low excitation energy required. The experimental Figure 5.18 confirms that atoms ‘D’ and ‘E’ flip at a bias voltage of ~ 2 mV, while the next atoms ‘F’ and ‘G’ flip at ~ 5 mV. Figure 5.17 and Figures 5.20 - 5.22 confirm that atoms ‘D’ and ‘E’ have flipped. Atoms ‘F’ and ‘G’ may have flipped at the same time, but there is no evidence in the measurements. From the figures it is visible that atoms ‘A’, ‘B’ and ‘C’ do not flip, which is consistent with the simulations. Rationale: As the measurement methods are limited to probing a single atom or a single line at a time, when it reaches D and E and causes them to flip, it will not be possible to see what atoms F and G are doing at the same time. The expectation from the simulation results is that they should flip as well. However, this cannot be confirmed in Figure 5.17.

Chapter 6

Conclusion and Outlook

A successful numerical simulator has been made to simulate spin structures based on Heisenberg model, anisotropy Hamiltonian and Zeeman effect. This is verified by the behaviour of the single atom and the trimer. The simulations, made by the simulator, on the intrinsic frustrated magnetic D7 at finite field show a low energy first excited state, where atoms 'D-E-F-G' have flipped.

Vertical atom manipulation on Cu_3AuN_2 works the same as on Cu_2N . A few methods were found that increased the success rate of vertical atom manipulation on the Cu_3AuN_2 surface. This increased the building rate from a single structure built in a month to multiple structures built in a single day.

Successfully engineered spin structures on a square lattice that contain intrinsic magnetic frustration, the D7 and D9.

The intrinsic frustrated D7 shows switching between two states, where atoms 'D' and 'E' have telegraphic noise in the measurements. This partially verifies the prediction made from the simulations on the frustrated systems.

A prediction was made for the excitation frequency for a trimer influenced by the tip and the simulations are being used in the lab.

Recommendations for future research:

1. Additional investigation of D7, whether atoms 'F' and 'G' are switching with atoms 'D' and 'E' as predicted by the simulation. Also taking the histograms at higher currents as the two Gaussians started to appear.
2. Future research on building would be to automate the procedure. Building takes a significant amount of time and automation will help alleviate that and also remove some of the human errors.
3. Future research on Frustration would be to investigate larger structures, the

D9 has two forms one has more weak antiferromagnetic couplings as shown in simulation and the other has more strong antiferromagnetic couplings.

4. For ESR, investigating if Fe adatoms show a change in tunnel current and experimenting with different kinds of magnetic atoms.

Acknowledgements

I would like to thank my supervisor J. Gobeil for guiding me through my master thesis and always making time to answer my questions. I would also like to thank A.F. Otte for providing me with an opportunity to do my master thesis and also taking the time explain important physics. Furthermore I would like to thank D. Coffey for the many helpful discussions and insights. I would like to thank the Ottelab group in general for making me feel welcome and making this an enjoyable journey.

Finally, I would like to thank my family who supported and pushed me to finish writing this thesis.

Bibliography

- [1] A. Spinelli, *QUANTUM MAGNETISM THROUGH ATOMIC ASSEMBLY*. PhD thesis, Delft University of Technology, 2015.
- [2] S. Baumann, W. Paul, T. Choi, C. Lutz, A. Ardavan, and A. Heinrich, “Electron paramagnetic resonance of individual atoms on a surface,” vol. 350, pp. 417–420, 10 2015.
- [3] D.-J. Choi, R. Robles, S. Yan, J. A. J. Burgess, S. Rolf-Pissarczyk, J.-P. Gauyacq, N. Lorente, M. Ternes, and S. Loth, “Building complex kondo impurities by manipulating entangled spin chains,” *Nano Letters*, vol. 17, no. 10, pp. 6203–6209, 2017. PMID: 28872317.
- [4] S. Loth, S. Baumann, C. P. Lutz, D. M. Eigler, and A. J. Heinrich, “Bistability in atomic-scale antiferromagnets,” *Science*, vol. 335, no. 6065, pp. 196–199, 2012.
- [5] L. Balents, “Spin liquids in frustrated magnets,” vol. 464, pp. 199–208, 03 2010.
- [6] P. Anderson, “Resonating valence bonds: A new kind of insulator?,” *Materials Research Bulletin*, vol. 8, no. 2, pp. 153 – 160, 1973.
- [7] P. W. ANDERSON, “The resonating valence bond state in La_2CuO_4 and superconductivity,” *Science*, vol. 235, no. 4793, pp. 1196–1198, 1987.
- [8] M. Neto, M. Ribeiro, B. Sanyal, A. Bergman, R. Muniz, O. Eriksson, and A. Klautau, “Complex magnetic structure of clusters and chains of ni and fe on pt(111),” vol. 3, p. 3054, 10 2013.
- [9] R. I. NEPOMECHIE, “A spin chain primer,” *International Journal of Modern Physics B*, vol. 13, no. 24n25, pp. 2973–2985, 1999.
- [10] B. Bryant, A. Spinelli, J. J. T. Wagenaar, M. Gerrits, and A. F. Otte, “Local control of single atom magnetocrystalline anisotropy,” *Phys. Rev. Lett.*, vol. 111, p. 127203, 2013.
- [11] P. Schiffer, “Magnetic frustration squeezed out,” *Nature*, vol. 420, pp. 35–, nov 2002.

- [12] J. Gobeil, D. Coffey, S. J. Wang, and A. F. Otte, “Large insulating nitride islands on Cu₃Au as a template for atomic spin structures,” *ArXiv e-prints*, July 2018.
- [13] X. Chen, Y.-S. Fu, S.-H. Ji, T. Zhang, P. Cheng, X.-C. Ma, X.-L. Zou, W.-H. Duan, J.-F. Jia, and Q.-K. Xue, “Probing superexchange interaction in molecular magnets by spin-flip spectroscopy and microscopy,” *Phys. Rev. Lett.*, vol. 101, p. 197208, Nov 2008.
- [14] M. A. Ruderman and C. Kittel, “Indirect exchange coupling of nuclear magnetic moments by conduction electrons,” *Phys. Rev.*, vol. 96, pp. 99–102, Oct 1954.
- [15] G. Binnig and H. Rohrer, “Scanning tunneling microscopy,” *Surface Science*, vol. 126, no. 1, pp. 236 – 244, 1983.
- [16] G. Binnig, H. Rohrer, C. Gerber, and E. Weibel, “Surface studies by scanning tunneling microscopy,” *Phys. Rev. Lett.*, vol. 49, pp. 57–61, Jul 1982.
- [17] G. Binnig, C. F. Quate, and C. Gerber, “Atomic force microscope,” *Physical Review Letters*, vol. 56, pp. 930–933, Mar. 1986.
- [18] J. Repp, G. Meyer, S. M. Stojković, A. Gourdon, and C. Joachim, “Molecules on insulating films: Scanning-tunneling microscopy imaging of individual molecular orbitals,” *Phys. Rev. Lett.*, vol. 94, p. 026803, Jan 2005.
- [19] A. J. Heinrich, J. A. Gupta, C. P. Lutz, and D. M. Eigler, “Single-atom spin-flip spectroscopy,” *Science*, vol. 306, no. 5695, pp. 466–469, 2004.
- [20] C. F. Hirjibehedin, C. P. Lutz, and A. J. Heinrich, “Spin coupling in engineered atomic structures,” *Science*, vol. 312, no. 5776, pp. 1021–1024, 2006.
- [21] F. Leibsle, S. Dhesi, S. Barrett, and A. Robinson, “Stm observations of cu(100)-c(2×2)_n surfaces: evidence for attractive interactions and an incommensurate c(2 × 2) structure,” *Surface Science*, vol. 317, no. 3.
- [22] C. F. Hirjibehedin, C.-Y. Lin, A. F. Otte, M. Ternes, C. P. Lutz, B. A. Jones, and A. J. Heinrich, “Large magnetic anisotropy of a single atomic spin embedded in a surface molecular network,” *Science*, vol. 317, no. 5842, pp. 1199–1203, 2007.
- [23] T. Choi, C. D. Ruggiero, and J. A. Gupta, “Incommensurability and atomic structure of c(2×2)_n/cu(100): A scanning tunneling microscopy study,” *Physical Review B*, vol. 78, jul 2008.
- [24] H. Niehus and C. Achete, “Surface structure investigation of nitrogen and oxygen on cu₃au(100),” vol. 289, no. 1, pp. 19–29.

- [25] S. Loth, C. P. Lutz, and A. J. Heinrich, “Spin-polarized spin excitation spectroscopy,” *New Journal of Physics*, vol. 12, no. 12, p. 125021, 2010.
- [26] W. Paul, S. Baumann, C. P. Lutz, and A. J. Heinrich, “Generation of constant-amplitude radio-frequency sweeps at a tunnel junction for spin resonance stm,” *Review of Scientific Instruments*, vol. 87, no. 7, p. 074703, 2016.
- [27] D. M. Eigler and E. K. Schweizer, “Eigler, d. m. & schweizer, e. k. positioning single atoms with a scanning tunneling microscope. nature 344, 524-526,” vol. 344, pp. 524–526, 04 1990.
- [28] S.-W. Hla, “Scanning tunneling microscopy single atom/molecule manipulation and its application to nanoscience and technology,” *Journal of Vacuum Science & Technology B: Microelectronics and Nanometer Structures Processing, Measurement, and Phenomena*, vol. 23, no. 4, pp. 1351–1360, 2005.
- [29] S. Rolf-Pissarczyk, S. Yan, L. Malavolti, J. A. J. Burgess, G. McMurtrie, and S. Loth, “Dynamical negative differential resistance in antiferromagnetically coupled few-atom spin chains,” *Phys. Rev. Lett.*, vol. 119, p. 217201, Nov 2017.